METHODS AND RESOURCES

A mutagenesis screen for essential plastid biogenesis genes in human malaria parasites

Yong Tang[1], Thomas R. Meister[2], Marta Walczak[1], Michael J. Pulkoski-Gross[1], Sanjay B. Hari[3], Robert T. Sauer[3], Katherine Amberg-Johnson[4], Ellen Yeh[1,4,5,6]*

1 Department of Biochemistry, Stanford University School of Medicine, Stanford, California, United States of America, 2 Department of Molecular and Cellular Physiology, Stanford University School of Medicine, Stanford, California, United States of America, 3 Department of Biology, Massachusetts Institute of Technology, Cambridge, Massachusetts, United States of America, 4 Department of Microbiology and Immunology, Stanford University School of Medicine, Stanford, California, United States of America, 5 Department of Pathology, Stanford University School of Medicine, Stanford, California, United States of America, 6 Chan Zuckerberg Biohub, San Francisco, California, United States of America

* ellenyeh@stanford.edu

Abstract

Endosymbiosis has driven major molecular and cellular innovations. *Plasmodium* spp. parasites that cause malaria contain an essential, non-photosynthetic plastid—the apicoplast—which originated from a secondary (eukaryote–eukaryote) endosymbiosis. To discover organellar pathways with evolutionary and biomedical significance, we performed a mutagenesis screen for essential genes required for apicoplast biogenesis in *Plasmodium falciparum*. Apicoplast(−) mutants were isolated using a chemical rescue that permits conditional disruption of the apicoplast and a new fluorescent reporter for organelle loss. Five candidate genes were validated (out of 12 identified), including a triosephosphate isomerase (TIM)-barrel protein that likely derived from a core metabolic enzyme but evolved a new activity. Our results demonstrate, to our knowledge, the first forward genetic screen to assign essential cellular functions to unannotated *P. falciparum* genes. A putative TIM-barrel enzyme and other newly identified apicoplast biogenesis proteins open opportunities to discover new mechanisms of organelle biogenesis, molecular evolution underlying eukaryotic diversity, and drug targets against multiple parasitic diseases.

Author summary

Plasmodium parasites, which cause malaria, and related apicomplexan parasites evolved from photosynthetic algae that acquired their chloroplast through two successive endosymbioses. Although no longer photosynthetic, the apicomplexan plastid—or apicoplast—was retained in these pathogens and provides critical metabolites during host cell infection. The apicoplast is of major interest for its unique biology and potential to yield new antimalarial drug targets. Here, we focused on the critical genes required to grow, divide, and inherit new apicoplasts during parasite replication. Given the apicoplast's divergent evolution, most of these cannot be recognized by their homology to genes with known functions. Instead, we overcame significant technical challenges in the *Plasmodium*

experimental system to perform an unbiased screen to search for these critical genes. Our screen has uncovered new genes with intriguing evolution and function that open up opportunities to understand and ultimately exploit apicoplast biology. Finally, assigning new, essential gene functions in *Plasmodium* parasites remains a daunting task. The successful identification of essential gene functions using an unbiased approach in this study provides a viable route for expansion of this screen or developing screens for other novel *Plasmodium* pathways in the future.

Introduction

Plasmodium spp., which cause malaria, and related apicomplexan parasites are important human and veterinary pathogens. These disease-causing protozoa are highly divergent from well-studied model organisms that are the textbook examples of eukaryotic biology, such that parasite biology often reveals striking eukaryotic innovations. The apicoplast, a nonphotosynthetic plastid found in apicomplexa, is one such "invention" [1, 2]. These intracellular parasites evolved from photosynthetic algae that acquired their plastids through secondary endosymbiosis [3]. During secondary endosymbiosis, a chloroplast-containing alga, itself the product of primary endosymbiosis, was taken up by another eukaryote to form a secondary plastid [4]. Despite the loss of photosynthesis in apicomplexans, the apicoplast contains several prokaryotic metabolic pathways, is essential for parasite replication during human infection, and is a target of antiparasitic drugs [5–8].

There are many traces of the apicoplast's quirky evolution in its present-day cell biology, in particular the pathways for its biogenesis. Like other endosymbiotic organelles, the single apicoplast cannot be formed de novo and must be inherited by its growth, division, and segregation into daughter cells. The few molecular details we have about apicoplast biogenesis hint at the major innovations that have occurred in the process of adopting and retaining this secondary plastid. The apicoplast is bound by four membranes acquired through successive endosymbioses, such that apicoplast proteins transit through the endoplasmic reticulum (ER) and use a symbiont-derived ER-associated degradation (ERAD)-like machinery (SELMA) to cross the two new outer membranes [9]. Curiously, autophagy-related protein 8 (Atg8), a highly conserved eukaryotic protein and key marker of autophagosomes, localizes to the apicoplast and is required for its inheritance in *Plasmodium* and the related apicomplexan parasite *Toxoplasma gondii* [10–12]. While SELMA and *Pf*Atg8 are clear examples of molecular evolution in action, other novel or repurposed proteins required for apicoplast biogenesis remain undiscovered.

So far, new apicoplast biogenesis proteins have primarily been discovered through candidate approaches. SELMA was first identified as homologs of the ERAD machinery encoded in the nucleomorph, the remnant nucleus of the eukaryotic symbiont found in some algal secondary plastids [13]. Nuclear-encoded versions of SELMA containing apicoplast-targeting sequences were then detected in the genomes of apicomplexan parasites (which lack a nucleomorph) [14]. Because the apicoplast proteome is enriched in proteins likely to perform biogenesis functions such as protein import or genome replication, several apicoplast-targeted proteins of unknown function have also been shown to be required for its biogenesis [15]. ATG8's novel apicoplast function was discovered serendipitously by its unexpected localization on the apicoplast instead of autophagosomes [10]. Though candidate approaches have yielded new molecular insight [16–18], in general they are indirect and may bias against novel pathways.

In blood-stage *Plasmodium falciparum*, a method to chemically rescue parasites that have lost the apicoplast has paved the way for functional screens [19–21]. Addition of isopentenyl diphosphate (IPP) to the growth media is sufficient to reverse growth inhibition caused by

apicoplast loss because it is the only essential metabolic product of the apicoplast in the blood stage. Taking advantage of the apicoplast chemical rescue, we recently took the first unbiased approach to discover a new apicoplast biogenesis protein [22]. We first screened for small-molecule inhibitors that specifically disrupt apicoplast biogenesis in *P. falciparum*. Subsequent target identification led us to a membrane metalloprotease, the *P. falciparum* ATP-dependent zinc metalloprotease 1 (*Pf*FtsH1), with an unexpected role in apicoplast biogenesis. This chemical genetic screen has the advantage of unbiased sampling of druggable targets in apicoplast biogenesis pathways. Unfortunately, it lacks throughput given the painstaking process of mapping inhibitors to their molecular targets.

Forward genetic screens are widely performed to uncover novel cellular pathways, such as those required for apicoplast biogenesis. Recently, genome-scale deletion screens performed in several apicomplexan parasites have uncovered a plethora of essential genes of unknown function [23–25]. Several challenges impede large-scale functional analysis of these essential genes. First, targeted gene modifications are still slow and labor intensive in *P. falciparum*, the most deadly of the human malaria species, despite an available in vitro blood culture system [26, 27]. Second, efficient methods for generating conditional mutants, such as RNA interference (RNAi) or Clustered Regularly Interspaced Palindromic Repeats interference (CRISPRi) systems, are lacking in all apicomplexan organisms [28]. Finally, high-throughput, single-cell phenotyping for important functions need to be developed [29]. Overcoming these significant limitations, we designed a forward genetic screen using chemical mutagenesis, apicoplast chemical rescue, and a fluorescent reporter for apicoplast loss to identify essential apicoplast biogenesis genes in blood-stage *P. falciparum*. The screen identified known and novel genes required for apicoplast biogenesis and is, to our knowledge, the first forward genetic screen to assign essential cellular functions in *P. falciparum*.

Results

A conditional fluorescent reporter enables single-cell phenotyping of apicoplast loss in *P. falciparum*

The apicoplast must be propagated during parasite replication, such that biogenesis defects result in newly replicated daughter parasites that do not contain an apicoplast. Because no clearance mechanism is known to eliminate the apicoplast in asexual blood-stage parasites, defective organelle biogenesis resulting in loss of inheritance is likely the major cause of apicoplast loss. To isolate rare *P. falciparum* mutants that have lost their apicoplast due to biogenesis defects, we set out to design a live-cell reporter for apicoplast loss. The apicoplast contains a prokaryotic caseinolytic protease (Clp) system composed of a Clp chaperone (ClpC) that recognizes and unfolds substrates and a Clp protease (ClpP) that degrades the recognized substrates [30–32]. We hypothesized that (1) in the presence of a functional apicoplast, ClpCP could be co-opted to degrade and turn "off" a fluorescent reporter, whereas (2) loss of the apicoplast would result in loss of ClpCP activity and therefore turn "on" the reporter (Fig 1A).

Clp substrates are typically recognized by unstructured degron sequences, the best studied of which is a transfer-messenger RNA (ssrA) that appends a short peptide to the C-terminus of translationally stalled proteins [33, 34]. However, the substrate specificity of the apicoplast ClpCP system has yet to be defined. Reasoning that the *Pf*ClpCP homolog might recognize similar degrons as bacterial or algal Clp systems, we tested two degrons recognized by *Escherichia coli* ClpXP—the *E. coli* ssrA peptide (*Ec*ssrA) and X7—and the predicted ssrA peptide in the red alga *Cyanidium caldarium*, *Cc*ssrA (S1 Table) [35–37]. To assess their functionality in *P. falciparum*, the C-terminus of an apicoplast-targeted green fluorescent protein (acyl-carrier protein leader peptide [ACP$_L$-GFP]) was modified with each of the degrons (Fig 1B). A
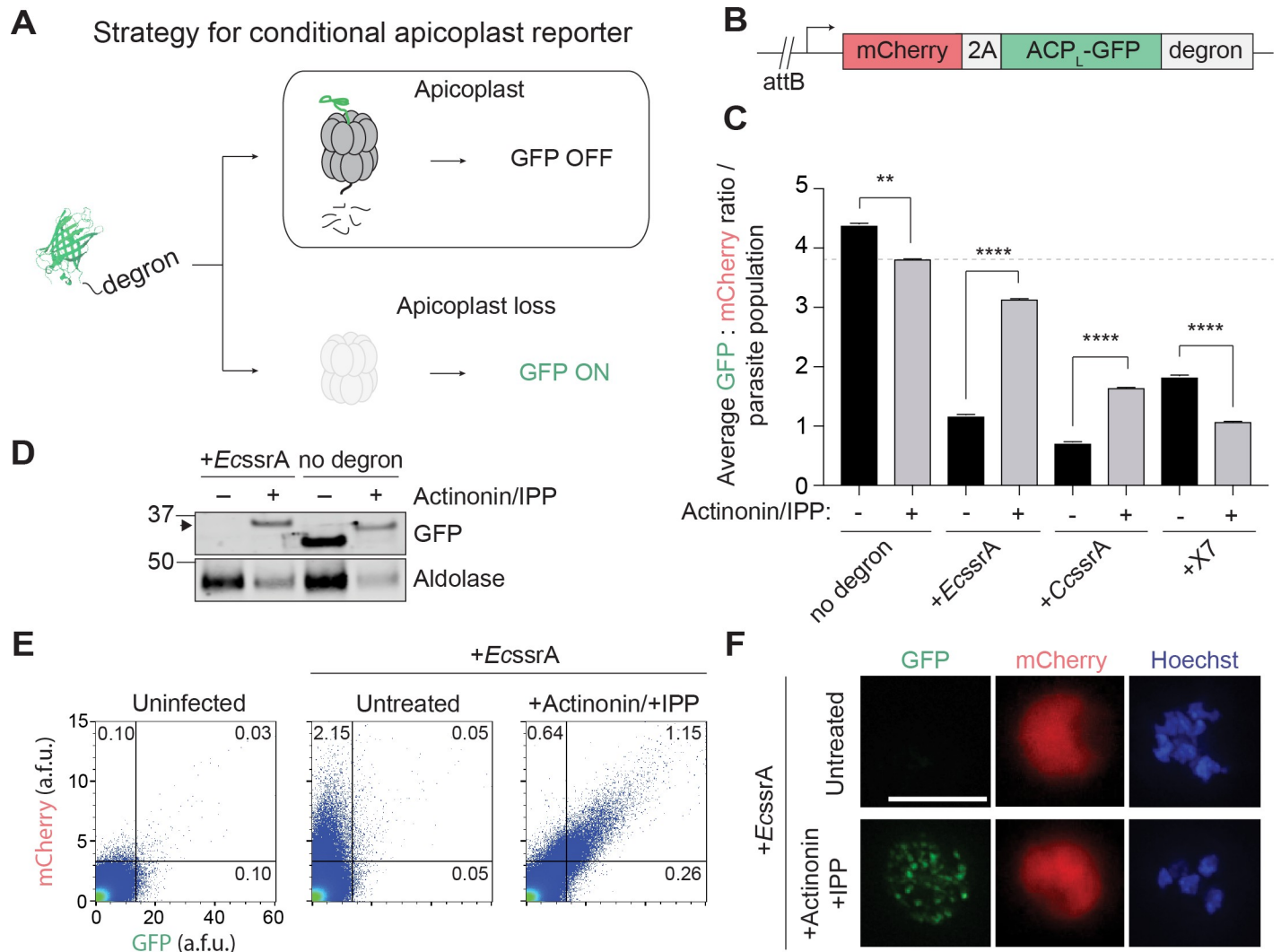
Fig 1. A fluorescent reporter for apicoplast loss in *P. falciparum* is specifically degraded in the apicoplast. (A) Strategy for a conditional GFP reporter that fluoresces upon apicoplast loss. (B) Reporter construct for expression of apicoplast-targeted GFP (ACP$_L$-GFP) and cytoplasmic mCherry used for integration into *P. falciparum* Dd2^{attB} parasites. (C) Ratio of GFP:mCherry fluorescence in untreated versus actinonin/IPP-treated parasites expressing ACP$_L$-GFP-degron. Data are shown as mean ± SEM ($n = 3$). ****$P < 0.0001$, unpaired two-tailed t test. See also S1 Fig. Tabulated data are shown in S1 Data. (D) GFP protein levels in untreated versus actinonin/IPP-treated parasites expressing GFP-*Ec*ssrA. Higher molecular weight species in GFP blot from unprocessed ACP$_L$ is indicated with black arrowhead. (E) Flow cytometry plots showing mCherry and GFP fluorescence in untreated versus actinonin/IPP-treated parasites expressing GFP-*Ec*ssrA. Uninfected RBCs are gated away (lower left quadrants), and the percentage mCherry$^+$, GFP$^+$ parasites in the gated populations relative to the total number of cells quantified are indicated. (F) Representative live-cell fluorescent images of untreated and actinonin/IPP-treated parasites expressing mCherry and GFP-*Ec*ssrA. Hoechst stains for parasite nuclei. Scale bar 5 μm. ACP, acyl-carrier protein; ACP$_L$, ACP leader peptide; a.f.u., arbitrary fluorescence units; *Ec*ssrA, *E. coli* ssrA peptide; GFP, green fluorescent protein; IPP, isopentenyl diphosphate; RBC, red blood cell.

cytosolic mCherry marker was also expressed on the same promoter as ACP$_L$-GFP via a T2A "skip" peptide to normalize apicoplast GFP levels to stage-specific promoter expression [38]. Each construct was then integrated into an ectopic *att*B locus in Dd2^{attB} parasites to generate the reporter strains [39].

For each reporter strain, the ratio of GFP:mCherry fluorescence (as detected by flow cytometry) was assessed in untreated parasites containing an intact apicoplast, designated apicoplast (+), and in parasites treated with actinonin (which causes apicoplast loss via inhibition of FtsH1) and rescued with IPP rendering them apicoplast(−). In the absence of a degron, the

GFP:mCherry ratio decreased modestly in apicoplast(−) parasites compared to apicoplast(+) (Fig 1C, S1 Fig and S1 Data). Though GFP was present in both populations, live fluorescence microscopy confirmed its localization to a branched structure characteristic of the apicoplast in apicoplast(+) parasites and to dispersed punctae as previously reported in apicoplast(−) parasites (S1 Fig) [19]. Addition of each of the three degrons to the C-terminus of ACP$_L$-GFP caused a 60%–84% decrease in the GFP:mCherry ratio in apicoplast(+) parasites, consistent with specific degradation of GFP (Fig 1C). In ACP$_L$-GFP-*Ec*ssrA and ACP$_L$-GFP-*Cc*ssrA populations, the GFP:mCherry ratio recovered to 88% and 44% relative to the ACP$_L$-GFP population in apicoplast(−) parasites, respectively (Fig 1C and 1E, S1 Fig and S1 Data). Unexpectedly, ACP$_L$-GFP-X7 populations showed further reduction of GFP:mCherry in apicoplast(−) parasites (Fig 1C, S1 Fig and S1 Data). Notably, cytoplasmic mCherry levels were similar between apicoplast(+) and apicoplast(−) parasites in all reporter strains, suggesting that the differences in GFP levels were not due to altered expression levels (S1 Fig and S1 Data). Of the 3 degrons tested, both the *Ec*ssrA and *Cc*ssrA peptide caused apicoplast-specific GFP degradation as designed.

We further characterized ACP$_L$-GFP-*Ec*ssrA because the greatest recovery of GFP fluorescence following apicoplast loss was observed with this reporter (Fig 1C). Consistent with degradation of GFP in the apicoplast being dependent on *Ec*ssrA peptide, ACP$_L$-GFP-*Ec*ssrA protein was detected at a significant level only in apicoplast(−) parasites, while unmodified ACP$_L$-GFP was detected in both apicoplast(+) and (−) parasites (Fig 1D). Of note, cleavage of the apicoplast-targeting ACP$_L$ sequence does not occur in apicoplast(−) parasites, resulting in an ACP$_L$-GFP protein of higher molecular weight compared to apicoplast(+) parasites [19]. Flow cytometry and live fluorescence microscopy confirmed that apicoplast(+) parasites displayed only cytosolic mCherry fluorescence, whereas apicoplast(−) parasites displayed both cytosolic mCherry and dispersed, punctate GFP fluorescence (Fig 1E and 1F). As expected, addition of IPP alone did not result in significant formation of apicoplast(−) parasites or recovery of ACP$_L$-GFP-*Ec*ssrA (S1 Fig and S1 Data). Taken together, these results demonstrate that ACP$_L$-GFP-*Ec*ssrA serves as a specific reporter for apicoplast loss in *P. falciparum*.

A phenotypic screen isolates a collection of apicoplast(−) mutant clones

Next, we used the ACP$_L$-GFP-*Ec*ssrA reporter strain to perform a phenotypic screen for apicoplast(−) mutants (Fig 2A). Ring-stage parasites were mutagenized with the alkylating agents ethyl methanesulfonate (EMS) or *N*-ethyl-*N*-nitrosourea (ENU) with the expectation that this would generate a more diverse population of parasites, some of which harbor mutations in apicoplast biogenesis genes rendering them apicoplast(−) [21, 22]. To rescue the lethality of apicoplast loss, mutagenized parasites were supplemented with 200 μM IPP in the growth media. A control group of non-mutagenized parasites was also cultured with IPP to assess whether apicoplast(−) mutants naturally occurred over time in the absence of selective pressure to maintain the organelle.

After two replication cycles to allow for initial apicoplast loss, mCherry-expressing parasites displaying GFP fluorescence greater than about 70% percentile were isolated by fluorescence-activated cell sorting (FACS). Selected mCherry(+) and GFP(+) parasites were then allowed to propagate to a detectable parasitemia before being subjected to another round of FACS. In one exemplary ENU-mutagenized population, a distinct population of GFP-positive parasites began to emerge after just two rounds of FACS (Fig 2B). Other populations showed enrichment beginning after three rounds of FACS. No significant enrichment of GFP signal was observed when parasites were (1) grown with IPP over time without FACS or (2) grown without IPP and subjected to FACS, suggesting that we specifically enriched for apicoplast(−)
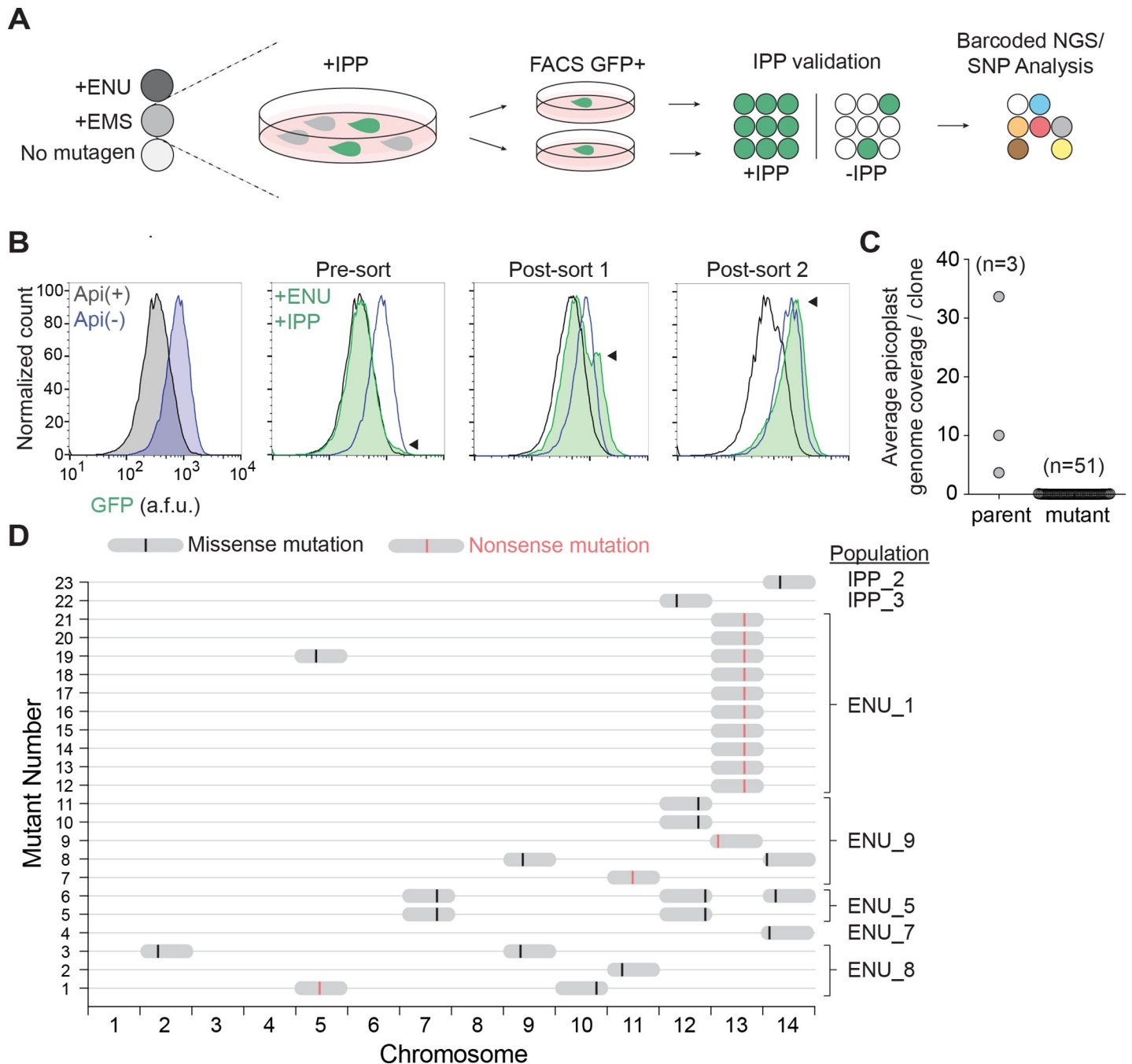
Fig 2. A screen for apicoplast(−) mutant clones identifies candidate biogenesis genes. (A) Schematic for selection and characterization of apicoplast(−) mutant clones. (B) Representative flow cytometry histograms of ENU_1 population (shown in D) GFP fluorescence over the course of successive fluorescence-activated cell sorts. Distribution of GFP fluorescence for pure populations of apicoplast(+) and apicoplast(−) parasites are shown for comparison in grey and blue, respectively. (C) Apicoplast genome coverage in parental strains and mutant clones from whole-genome sequencing. Tabulated data are shown in S2 Data. (D) Genomic loci of SNVs identified in coding regions of mutant clones. The mutagenized populations from which each clone was derived are indicated. For specific mutations, see also Table 1 and S2 Table. a.f.u., arbitrary fluorescence units; EMS, ethyl methanesulfonate; ENU, *N*-ethyl-*N*-nitrosourea; FACS, fluorescence-activated cell sorting; GFP, green fluorescent protein; IPP, isopentenyl diphosphate; NGS, next generation sequencing; SNP, single nucleotide polymorphism; SNV, single nucleotide variant.

mutants. Parasites from the final enriched apicoplast(−) populations were individually sorted

to generate apicoplast(−) clones derived from single parasites. Each clonal population was then re-checked for IPP-dependent growth and GFP fluorescence.

Whole-genome sequencing identifies 12 candidate genes required for apicoplast biogenesis

To determine the genetic basis of apicoplast loss, we sequenced the genomes of 51 apicoplast (−) clones (mutagenized = 40; non-mutagenized = 11) and three parent populations. Sequenced reads were mapped to the genome of *P. falciparum* 3D7 (version 35) with an average read depth of 26 for all samples. Notably, while the apicoplast genome was sequenced at an average depth of 16 reads in the parent populations, it was only detected with an average of 0.02 reads in apicoplast(−) clones (Fig 2C and S2 Data). Because the organellar genome is a marker for the apicoplast, the absence of the apicoplast genome confirmed the loss of the apicoplast in the sequenced clones [19, 22].

We next performed single nucleotide variant (SNV) analysis. A raw variant list was generated for each sample by comparison to the reference 3D7 genome and included SNVs found in parent populations at ≥5% allele frequency (minimum one read), and in apicoplast(−) clones at ≥90% (minimum five reads). Any SNV identified in apicoplast(−) clones that was also identified in any of the three parent populations was removed. We also filtered out SNVs detected in noncoding regions or resulting in synonymous amino acid changes in coding regions. Finally, SNVs identified in hypervariable regions of the genome (including the *rifin*, *stevor*, and *EMP* gene families) and/or previously annotated in the PlasmoDB single nucleotide polymorphism (SNP) database were excluded. After these filtering steps, 23 apicoplast(−) clones had at least one but no more than three SNVs that differed from the parent populations (Fig 2D; S2 Table).

Because genes required for apicoplast biogenesis ought to be essential, we used essentiality data from literature or whole-genome deletion screens performed in blood-stage *P. falciparum* and *P. berghei* to prioritize gene candidates [24, 25]. Of 18 unique SNVs identified, 12 were in genes categorized as "essential" in blood-stage *P. falciparum* and/or *P. berghei* (Table 1 and S2 Table). Although *Pf*FtsH1 (Pf3D7_1239700) is categorized as "dispensable" in the *P. falciparum* deletion screen, it has been shown experimentally to be essential [25]. Overall, a mutation in one of these 12 essential gene candidates was identified in each of the 23 apicoplast(−) clones, consistent with the mutation causing apicoplast loss. Potentially disruptive mutations included a I437S variant in the known apicoplast biogenesis protein (*Pf*FtsH1), truncation of Atg7 (*Pf*Atg7) likely required for a cytoplasmic pathway for apicoplast biogenesis, and truncations of three proteins of unknown function (Pf3D7_0518100, Pf3D7_1305100, and Pf3D7_1363700) (Table 1). The remaining candidates contained point mutations and had no known prior function in apicoplast biogenesis or localization to the organelle.

The Ile437Ser variant causes loss of *Pf*FtsH1 activity in vitro

*Pf*FtsH1 is an apicoplast membrane metalloprotease that was previously identified in a chemical genetic screen as the target of actinonin, an inhibitor that disrupts apicoplast biogenesis. Subsequent knockdown of *Pf*FtsH1demonstrated that it is required for apicoplast biogenesis [22]. We hypothesized that the I437S variant identified in our screen disrupted *Pf*FtsH1 function, leading to apicoplast loss. *Pf*FtsH1 contains both an ATPase and peptidase domain. To test the effect of I437S on enzyme activity, we compared the activity of I437S with that of wild-type (WT) enzyme, an ATPase-inactive E249Q variant, and a peptidase-inactive D493A variant (Fig 3A). All enzymes were purified without the transmembrane domain as previously described (S3 Fig) [22].

Table 1. List of top candidate genes from screen.

Gene ID	Annotation	Variant	Essential in *P. falciparum* piggyBac screen[a]	Essential in *P. berghei* screen[b]	Essential in other literature
Pf3D7_1239700	ATP-dependent zinc metalloprotease FtsH1	Ile437Ser	No	ND	Yes[c]
Pf3D7_1126100	Atg7, putative	Gln719*	Yes	ND	Yes[d]
Pf3D7_0518100	RAP protein, putative	Leu1419*	No	Yes	ND
Pf3D7_1305100	Conserved *Plasmodium* protein, unknown function	Lys859*	Yes	ND	ND
Pf3D7_1363700	Conserved *Plasmodium* protein, unknown function	Tyr4669*	Yes	Yes	ND
Pf3D7_0913500	Protease, putative	Ser347Gly	Yes	ND	ND
Pf3D7_1408700	Conserved *Plasmodium* protein, unknown function	Ile4809Val	No	Yes	ND
Pf3D7_1114900	Conserved *Plasmodium* protein, unknown function	Lys932Ile	Yes	Yes	ND
Pf3D7_0910100	Exportin-7, putative	Ser102Pro	Yes	Yes	ND
Pf3D7_1417800	DNA replication licensing factor MCM2	Thre584Ile	Yes	Yes	ND
Pf3D7_1433800	Conserved *Plasmodium* protein, unknown function	Asp431Val	Yes	ND	ND
Pf3D7_1203300	Conserved *Plasmodium* protein, unknown function	Lys473Thr	Yes	ND	ND

[a]From *P. falciparum* piggyBac screen dataset [25].

[b]From *P. berghei* deletion screen dataset [24].

[c]From [22].

[d]From [40].

*Stop codon.

Candidates were prioritized based on previous literature suggesting an apicoplast function (first group) and presence of a nonsense mutation (second group). The remaining candidates were unranked. Note that the first two digits of the Pf gene ID indicate the chromosome on which the gene is located.

Abbreviations: Atg7, autophagy-related protein 7; FtsH1, ATP-dependent zinc metalloprotease 1; MCM, minichromosome maintenance; ND, not determined; RAP, RNA-binding domain abundant in Apicomplexans.

https://doi.org/10.1371/journal.pbio.3000136.t001

We first measured peptidase activity on a fluorescent casein substrate. Neither the I437S nor the D493A variant had detectable peptidase activity, whereas WT enzyme turned over substrate at 0.4 min^{-1} (Fig 3B, S3 Table and S3 Data). Similarly, the I437S and E249Q variants showed no detectable ATP hydrolysis activity, in contrast to both WT and the D493A variants (Fig 3C, S3 Table and S3 Data). Taken together, these results validate the identified missense mutation leading to expression of inactive *Pf*FtsH1 I437S variant as causative for apicoplast loss.

*Pf*Atg7, a member of the Atg8 conjugation pathway, is a cytoplasmic protein required for apicoplast biogenesis

Though non-apicoplast proteins are expected to play a role in apicoplast biogenesis, all apicoplast biogenesis proteins validated so far have localized to the apicoplast because this criterion is most often used to select candidates. A significant advantage of our forward genetic screen is that it can uncover non-apicoplast pathways required for apicoplast biogenesis, which are biased against by other approaches. A cytoplasmic protein strongly identified in our screen was *Pf*Atg7 (Pf3D7_1126100), which contained a nonsense mutation causing a protein truncation at position Q719. The premature stop codon was upstream of the E1-like activating domain, consistent with *Pf*Atg7 loss of function (Fig 4A). In yeast and mammalian cells, Atg7
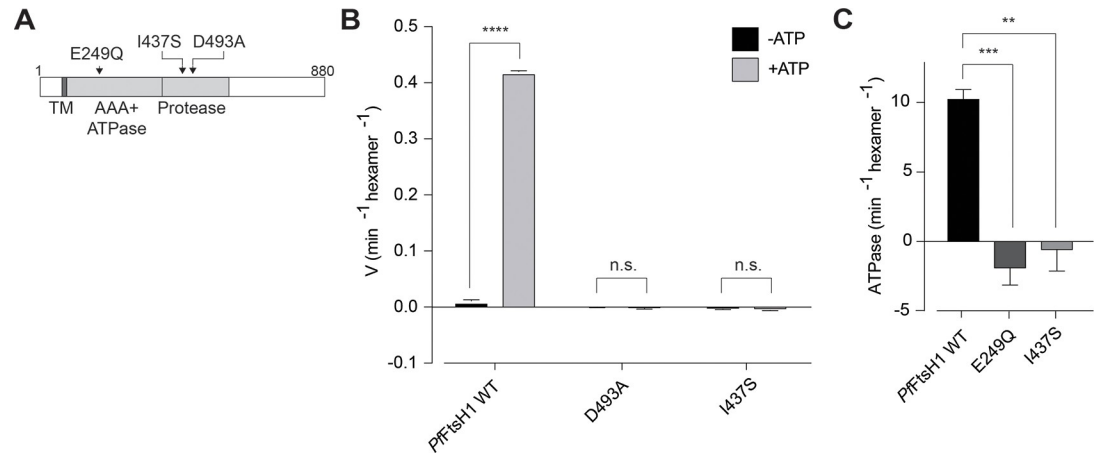
Fig 3. The I437S variant disrupts *Pf*FtsH1 protease and ATPase activity in vitro. (A) Domain organization of *Pf*FtsH1 showing location of I437S. The known ATPase-inactive (E249Q) and peptidase-inactive (D493A) variants are also shown. (B) Peptidase activity of recombinant *Pf*FtsH1 WT and mutants. Data are shown as mean ± SEM ($n = 3$). ****$P < 0.0001$, unpaired two-tailed t test. Tabulated data are shown in S3 Data. (C) ATPase activity of recombinant *Pf*FtsH1 WT and mutants. Data are shown as mean ± SEM ($n = 3$). ***$P = 0.0009$, **$P = 0.0016$ adjusted P values compared to WT, ordinary one-way ANOVA with Tukey's multiple comparisons test. Tabulated data are shown in S3 Data. *Pf*FtsH1, *P. falciparum* ATP-dependent zinc metalloprotease 1; TM transmembrane; V, velocity; WT, wild-type.

https://doi.org/10.1371/journal.pbio.3000136.g003

is required for conjugation of Atg8 to the autophagosome membrane [41]. *Pf*Atg7 has not specifically been implicated in apicoplast biogenesis; however, *Pf*Atg8 has been shown to localize to the apicoplast membrane and be required for apicoplast biogenesis. In analogy with its role in autophagy, *Pf*Atg7 is likely required for conjugating *Pf*Atg8 to the apicoplast membrane. Therefore, we suspected the loss-of-function mutant we identified caused apicoplast loss via loss of membrane-conjugated *Pf*Atg8 [12].

To confirm *Pf*Atg7's role in apicoplast biogenesis, we generated a *P. falciparum* strain in which it is conditionally expressed. The endogenous *Pf*Atg7 locus in a NF54 strain harboring a CRISPR cassette was modified with a C-terminal triple hemagglutinin (HA) tag and a 3′ untranslated region (UTR) RNA aptamer sequence that binds a tetracycline repressor (TetR) and development of zygote inhibited (DOZI) fusion protein to generate *Pf*Atg7-TetR/DOZI [42, 43]. In the presence of anhydrotetracycline (ATc), the 3′UTR aptamer is unbound, and *Pf*Atg7-3×HA protein was detectable, albeit at low levels consistent with its low expression in published transcriptome data (PlasmoDB.org) (S2 Fig). Removal of ATc causes binding of the TetR/DOZI repressor, which resulted in undetectable *Pf*Atg7 protein levels by western blot within one replication cycle (S2 Fig). Immunofluorescence of HA-tagged *Pf*Atg7 showed diffuse cytoplasmic localization in the presence of ATc and overall reduction of fluorescence signal upon removal of ATc (S4 Fig). Parasitemia also decreased over the course of several replication cycles, consistent with a previous study showing that *Pf*Atg7 is essential (Fig 4B and S4 Data) [40].

We tested whether the requirement for *Pf*Atg7 was due to its role in apicoplast biogenesis. Growth inhibition caused by *Pf*Atg7 knockdown was partially rescued by addition of IPP (Fig 4B and S4 Data). Furthermore, in −ATc/+IPP parasites, the apicoplast marker acyl-carrier protein (ACP) mislocalized from a discrete organellar localization to multiple cytoplasmic puncta, a hallmark of apicoplast loss (Fig 4C) [19]. Loss of transit peptide cleavage of the apicoplast protein ClpP also confirmed apicoplast loss, because mislocalized apicoplast proteins do not undergo removal of their targeting sequences (Fig 4D) [15, 44]. IPP rescue of *Pf*Atg7 knockdown parasites was incomplete, raising the possibility that *Pf*Atg7 is also required for a non-
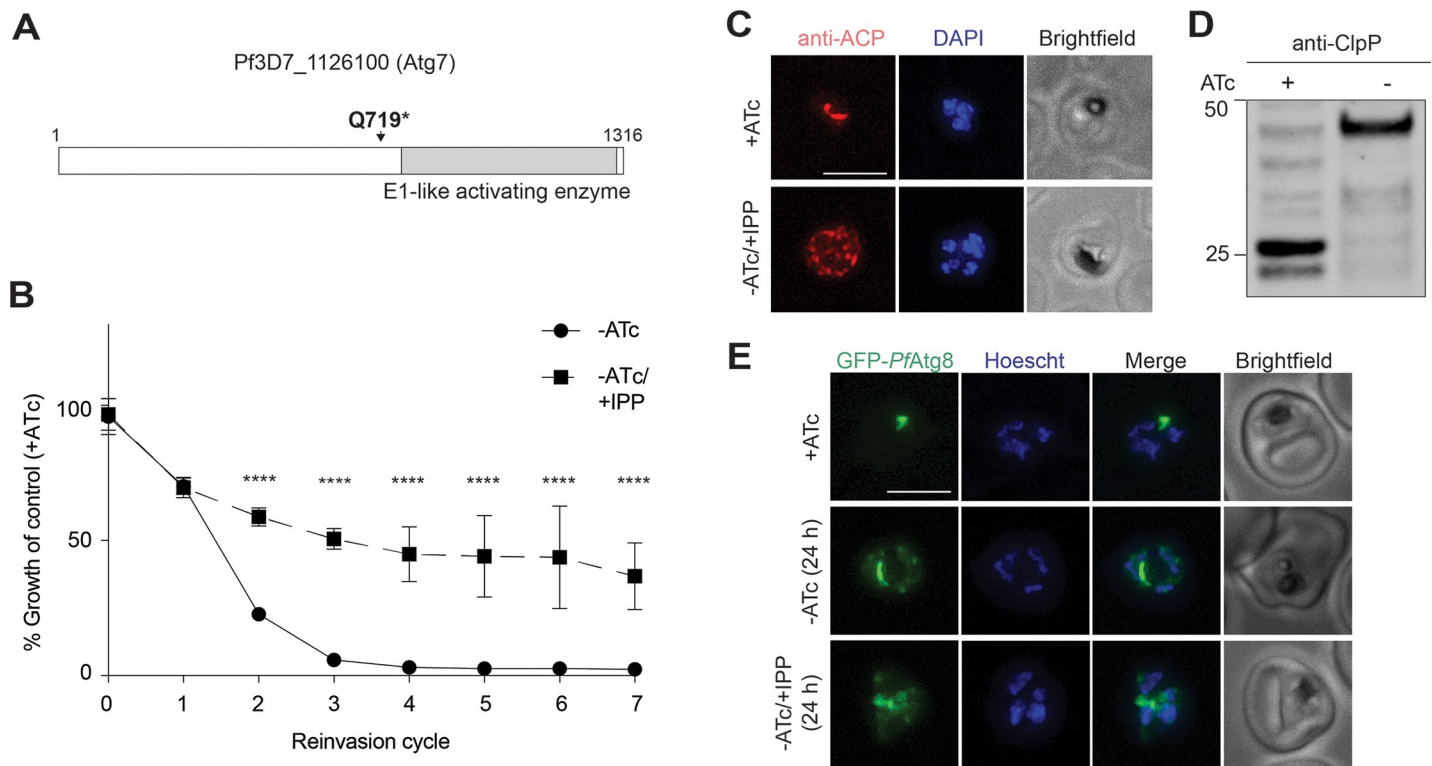
Fig 4. *Pf*Atg7 is a cytoplasmic protein required for *Pf*Atg8 membrane conjugation and apicoplast biogenesis. (A) Domain organization of *Pf*Atg7 showing location of the identified stop codon. (B) Growth time course of *Pf*Atg7-TetR/DOZI knockdown parasites in the absence of ATc with and without IPP. Data are shown as mean ± SD (n = 3). ****$P < 0.0001$ adjusted P value (−ATc compared to −ATc/+IPP), two-way ANOVA with Sidak's multiple comparisons test. Tabulated data are shown in S4 Data. (C) Representative immunofluorescence images of *Pf*Atg7-TetR/DOZI parasites showing apicoplast morphology (anti-ACP) in +ATc and −ATc/+IPP parasites at reinvasion cycle 7. Scale bar 5 μm. (D) Western blot of apicoplast-targeted ClpP in *Pf*Atg7-TetR/DOZI parasites in the presence and absence of ATc at reinvasion cycle 7. Processed ClpP after removal of its transit peptide is approximately 25 kDa, while full-length protein is about 50 kDa. Result is representative of n = 2 blots. (E) Live-cell fluorescent images of GFP-*Pf*Atg8 upon *Pf*Atg7 knockdown 24 hours post ATc removal, prior to apicoplast loss. Scale bar 5 μm. ACP, acyl-carrier protein; ATc, anhydrotetracycline; Clp, caseinolytic protease; ClpP, Clp protease; GFP, green fluorescent protein; IPP, isopentenyl diphosphate; *Pf*Atg7, *P. falciparum* autophagy-related protein 7; TetR/DOZI, tetracycline repressor/development of zygote inhibited fusion protein.

https://doi.org/10.1371/journal.pbio.3000136.g004

apicoplast function. Alternatively, *Pf*Atg7 knockdown may cause stalling of apicoplast morphologic development leading to general cellular toxicity that cannot be fully rescued with IPP until apicoplast loss is complete. To test these models, instead of *Pf*Atg7 knockdown followed by apicoplast loss, we first induced apicoplast loss with actinonin and then assessed the effects of *Pf*Atg7 knockdown. *Pf*Atg7 knockdown in apicoplast(−) parasites did not cause any additional growth defect and was fully rescued by IPP, suggesting that the partial rescue observed in apicoplast(+) parasites was due to the order of disruption (S5 Fig and S4 Data). These results confirmed that *Pf*Atg7 is required for apicoplast biogenesis and likely is its only essential function.

Finally, to determine whether *Pf*Atg7's role in apicoplast biogenesis was via *Pf*Atg8 membrane conjugation, we transfected *Pf*Atg7-TetR/DOZI with a transgene encoding GFP-*Pf*Atg8. In this strain, GFP-*Pf*Atg8 primarily localized to a branched structure in schizonts, consistent with its previously described apicoplast localization (Fig 4E) [10, 45]. Upon *Pf*Atg7 knockdown, GFP-*Pf*Atg8 localization to this discrete structure was lost, and accumulation in the cytoplasm was observed within a single replication cycle prior to apicoplast loss (Fig 4E). This result suggests that, like yeast and mammalian Atg7 homologs, *Pf*Atg7 has a conserved function in conjugating Atg8 to lipids. Altogether, *Pf*Atg7 stood out as a cytoplasmic protein required for apicoplast biogenesis identified in our screen.

Forward genetics identifies three "conserved *Plasmodium* proteins of unknown function" required for apicoplast biogenesis

The real power of forward genetics is the ability to uncover novel pathways without any a priori knowledge. Therefore, we next turned our attention to the nearly 50% of the *Plasmodium* genome annotated as "conserved *Plasmodium* protein, unknown function." Three candidate genes (Pf3D7_0518100, Pf3D7_1305100, and Pf3D7_1363700) encoding proteins of unknown function were identified by nonsense mutations that caused protein truncation. The position of the premature stop codon near the 5′ end (Pf3D7_0518100, Pf3D7_1305100) or in the middle (Pf3D7_1363700) of the genes suggested that these were loss-of-function mutations (Fig 5A). Incidentally, all were also identified in a recently published proteomic dataset of apicoplast proteins, and immunofluorescence colocalization with the apicoplast marker ACP confirmed that Pf3D7_0518100 and Pf3D7_1305100 are localized to the apicoplast (S4 Fig) [15].

Therefore, we assessed whether knockdown of these genes disrupted apicoplast biogenesis. Similar to the experiments performed to validate *Pf*Atg7, ATc-regulated knockdown strains for each of the candidate genes were generated. Upon ATc removal, protein levels for each gene decreased within 24 hours as detected by western blot (S2 Fig). Significant growth inhibition was also observed for all candidate genes tested, with varying kinetics of growth inhibition observed for each candidate (Fig 5B, 5E and 5H and S4 Data). Of note, the gene essentiality demonstrated here for Pf3D7_1305100 and Pf3D7_1363700 confirmed whole-genome essentiality data reported in *P. berghei* and/or *P. falciparum*. However, the essentiality of Pf3D7_0518100 did not agree with its "dispensable" annotation in the *P. falciparum* dataset. IPP supplementation reversed growth inhibition for all the candidates, demonstrating that their essentiality was due to an apicoplast-specific function (Fig 5B, 5E and 5H and S4 Data). Finally, mislocalization of ACP and loss of transit peptide cleavage of ClpP confirmed apicoplast loss for all candidates (Fig 5C, 5D, 5F, 5G, 5I and 5J). Because these genes have so far lacked any functional annotation and given their shared knockdown phenotype, we designated them "apicoplast-minus, IPP-rescued" (*amr*) genes: *amr1* (Pf3D7_1363700), *amr2* (Pf3D7_0518100), and *amr3* (Pf3D7_1305100). Taken together, we successfully identified three novel proteins of unknown function required for apicoplast biogenesis, prioritizing these *amr* genes for functional studies.

Sequence analysis of AMR1 homologs suggests gene duplication followed by evolution of a new function in apicoplast biogenesis

To set up future functional studies, we noted that *Pf*AMR1 contained a TIM-barrel domain with closest homology to indole-3-glycerol phosphate synthase (IGPS), a highly conserved enzyme in the tryptophan (trp) biosynthesis pathway [46–48]. This was surprising because *Plasmodium* and the related apicomplexan parasite *Toxoplasma* are trp auxotrophs [49–51]. Indeed, analysis of >30 apicomplexan genomes did not detect any of the other six trp biosynthetic enzymes, except the terminal enzyme tryptophan synthase (TS)-β, which was horizontally transferred into *Cryptosporidium* spp. [52]. Therefore, we suspected that *Pf*AMR1 may have a function unrelated to trp biosynthesis.

To test the conservation of active-site residues, we aligned the sequences of several known IGPSs with IGPS homologs identified from *P. falciparum*, *T. gondii*, and *Vitrella brassicaformis* (S6 Fig) [53–55]. *V. brassicaformis*, a member of the Chromerids, is the closest free-living, photosynthetic relative to apicomplexan parasites. It contains a secondary plastid with the same origin as the apicoplast but, as a free-living alga [56], is also expected to have intact trp biosynthesis. Known catalytic and substrate binding residues based on enzyme structure-function studies performed in bacteria were first identified [57]. For known IGPSs and one of the *V.*
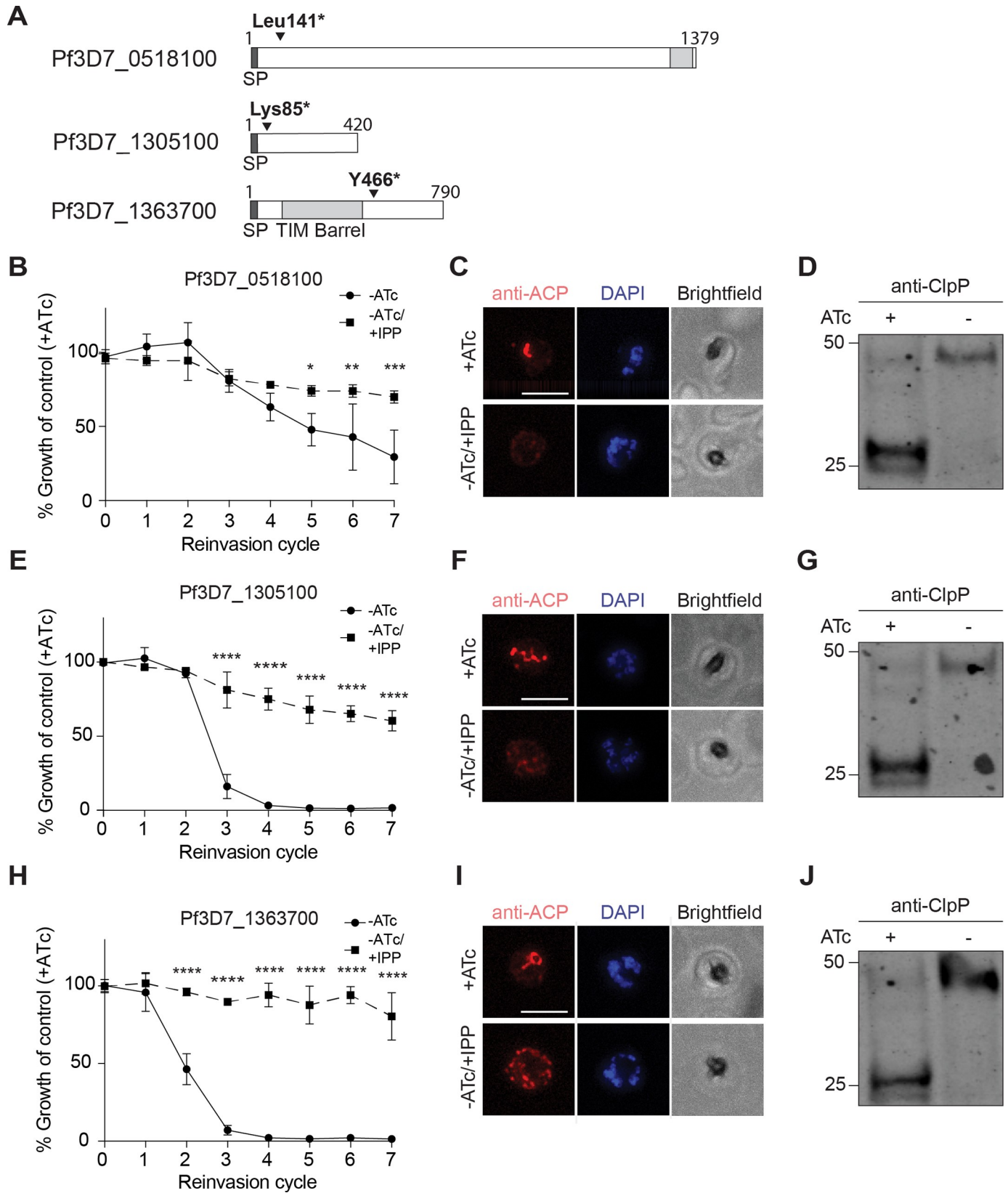
Fig 5. Three "conserved *Plasmodium* proteins of unknown function" are required for apicoplast biogenesis. (A) Domain organization of Pf3D7_0518100, Pf3D7_1305100, and Pf3D7_1363700 showing location of identified stop codons. (B, E, and H) Growth time course of Pf3D7_0518100, Pf3D7_1305100, and Pf3D7_1363700-TetR/DOZI knockdown parasites in the absence of ATc with and without IPP. Data are shown as mean ± SD (n = 3). $^{****}P < 0.0001$ adjusted P value (−ATc compared to −ATc/+IPP), two-way ANOVA with Sidak's multiple comparisons test. Tabulated data are shown in S4 Data. (C, F, and I) Representative immunofluorescence images of indicated TetR/DOZI parasites showing the apicoplast (anti-ACP) in +ATc and −ATc/+IPP parasites at reinvasion cycle 7. Scale bars 5 μm. (D, G, and J) Western blot of apicoplast-targeted ClpP in indicated TetR/DOZI parasites in the presence and absence of ATc at reinvasion cycle 7. Processed ClpP after removal of its transit peptide is approximately 25 kDa, while full-length protein is about 50 kDa. Results are representative of n = 2 western blots. ACP, acyl-carrier protein; ATc, anhydrotetracycline; Clp, caseinolytic protease; ClpP, Clp protease; IPP, isopentenyl diphosphate; TetR/DOZI, tetracycline repressor/development of zygote inhibited fusion protein.

https://doi.org/10.1371/journal.pbio.3000136.g005

brassicaformis IGPS homologs (Vbra_4894), the key catalytic and substrate binding residues were all conserved, despite the vast evolutionary distance between bacteria, metazoans, and Chromerids/apicomplexans (Fig 6A). However, in *Pf*AMR1 and the other two *V. brassicaformis* homologs, key functional residues were not conserved. Based on the conservation of functional residues, we separated these sequences into two groups: "canonical IGPS proteins" (which have been shown, or are likely, to encode for IGPS activity) and "IGPS-like proteins" (e.g., *Pf*AMR1), which we suggest have functionally diverged.

We next looked at the pattern of canonical IGPS versus IGPS-like proteins through two biological transitions: loss of trp biosynthesis (*Vitrella* versus *Plasmodium* spp.) and loss of the apicoplast (*Plasmodium* versus *Cryptosporidium* spp.) (Fig 6B). As expected for a role in trp biosynthesis, canonical IGPS proteins were retained until the emergence of parasitism. In addition, genes encoding the remaining set of enzymes for trp biosynthesis were identified in the *V. brassicaformis* genome [58]. Unlike canonical IGPSs, however, IGPS-like proteins were retained in parasites that have lost trp biosynthesis. Instead, loss of IGPS-like proteins is associated only with loss of the apicoplast in *Cryptosporidium* spp. This pattern of acquisition and loss of IGPS-like proteins suggests an apicoplast-specific function separate from trp biosynthesis.

Finally, we performed functional complementation to test the biochemical activity of canonical IGPS and IGPS-like genes from *V. brassicaformis* and *P. falciparum*. An *E. coli* strain (*trpC9800*) containing an inactivating mutation in trpC, the *E. coli* IGPS homolog, was grown on minimal agar (M9) [59]. As expected, *trpC9800* was dependent on trp supplementation for growth (Fig 6C). Complementation with the Vbra_4894 homolog restored *trpC9800* growth on M9, comparable to that of an *E. coli* strain with intact trp biosynthesis, suggesting that Vbra_4894 is an IGPS protein (Fig 6D). In contrast, neither *Pf*AMR1 nor any of the IGPS-like genes were able to functionally replace trpC, supporting an alternative biochemical function. Because glutathione S-transferase (GST)-tagged complemented protein could not be detected in any strain, we cannot rule out that the lack of functional complementation was due to differential protein expression or solubility below the detection limit of western blot. However, isopropyl β-D-1-thiogalactopyranoside (IPTG) induction of protein expression was toxic for all complemented strains, suggesting all constructs supported protein expression. Overall, we propose that AMR1 has evolved a new biochemical function required for apicoplast biogenesis.

Discussion

Apicoplast biogenesis provides a fascinating window into molecular evolution, including examples of proteins that have been reused (e.g., translocon on the inner chloroplast membrane/translocon on the outer chloroplast membrane [TIC/TOC] complexes) [17, 60, 61], repurposed (e.g., Atg8, symbiont-derived ERAD-like machinery [SELMA]) [12, 14], or newly invented in the process of serial endosymbioses. Overcoming significant technical challenges in the *Plasmodium* experimental system, we designed a forward genetic screen to identify

A

	canonical IGPS			IGPS-like		
Active site	*E. coli* (trpC)	*S. cerevisiae* (trpG)	*V. brassicaformis* (Vbra_4894)	*V. brassicaformis* (Vbra_5810)	*V. brassicaformis* (Vbra_14040)	*P. falciparum* (Pf3D7_1363700)
Ribulose[d]	E53	E273	E59	E717	D91	E242
Phosophate/Ribulose[d]	K55	K275	K61	M719	K93	K244
Anthranilate	P59	P279	P65	P723	P97	I248
Indole	F93	F314	F100	Y762	W137	T288
Ribulose/Indole[d]	K114	K343	K121	S783	K167	D316
Indole	F116	F345	F123	I785	L169	I318
Indole	M137	I366	I144	V806	N190	N339
Ribulose[d]	E163	E392	E159	S832	E215	E364
Ribulose[d]	N184	N413	N180	N854	N236	N385
Anthranilate	R186	R415	R182	L856	W238	Y387
Anthranilate/Indole	L188	L417	L184	F858	R240	F389
Phosphate	G216	G445	G212	G892	G268	N417
Phosphate	G236	G466	G233	S913	G289	E438

B

Trp pathway

C

M9 + carb + trp

D

M9 + carb

Fig 6. Evolutionary divergence from IGPS proteins suggests a novel apicoplast biogenesis function for *Pf*AMR1. (A) Conservation of active-site residues between IGPS and IGPS-like proteins. Sequences of IGPS homologs identified in *V. brassicaformis* and *P. falciparum* and known IGPS enzymes from *E. coli* and *Saccharomyces cerevisiae* were aligned. Active-site residues identified from structure-function studies in IGPS enzymes are listed. [d]Catalytic residues. See also S6 Fig. (B) Schematic of IGPS and IGPS-like protein loss in *P. falciparum* and *Cryptosporidium parvum*, respectively. (C) Complementation of an *E. coli* trpC mutant (*trpC9800*) with IGPS and IGPS-like proteins from *V. brassicaformis* and *P. falciparum* grown on minimal media (M9) + antibiotic resistance (carbenicillin) + and trp. Empty vector condition contains only antibiotic resistance. *BL21 Star (DE3)* strain was used for the WT condition. (D) Same complementation as in panel C but grown without trp. AMR, apicoplast-minus IPP-rescued; AS, anthranilate synthase;

IGPS, indole-3-glycerol phosphate synthase; IPP, isopentenyl diphosphate; PRT, phosphoribosyltransferase; trp, tryptophan; TS, tryptophan synthase; WT, wild-type.

essential apicoplast biogenesis pathways. This singular screen opens up opportunities to discover evolutionary innovations obscured by candidate-based approaches, including cytoplasmic pathways and genes lacking any functional annotations. In addition to confirming the role of *Pf*FtsH1 in apicoplast biogenesis and identification of *Pf*Atg8 conjugation machinery, we identified several proteins of unknown function required for apicoplast biogenesis that have so far gone undetected. Because our reporter specifically looked for apicoplast loss, we cannot rule out the possibility that some identified genes may be involved in maintenance of already formed apicoplasts. However, because no clearance mechanism is known for defective apicoplasts, we are not aware of any pathway by which defective apicoplasts would lead to organelle loss independent of parasite replication.

One surprising gene we identified was *Pf*AMR1, which encodes a TIM-barrel domain found in diverse enzymes catalyzing small-molecule reactions [46]. *Pf*AMR1 may have evolved from gene duplication of IGPS, an enzyme in the trp biosynthetic pathway [47]. However, the evolutionary pattern of retention in apicomplexan parasites lacking tryptophan biosynthesis and loss in *Cryptosporidium* spp., concomitant with plastid loss, supports a critical function of *Pf*AMR1 in the apicoplast independent of tryptophan biosynthesis. We hypothesize that *Pf*AMR1 may be involved in biosynthesis of a specialized lipid or signaling molecule required specifically for building new plastids in this lineage. Multiple new *amr* genes identified in this study provide striking examples of the unexpected findings enabled by unbiased screens.

Uncovering novel apicoplast biogenesis pathways also has important biomedical applications. While targeting the metabolic function of the apicoplast has been a major strategy for antimalarial drug discovery [62], it has become apparent that apicoplast biogenesis is equally as, or likely more, valuable as a therapeutic target [22]. These distinct pathogen pathways are nonetheless required in every proliferative stage of the *Plasmodium* life cycle and conserved among apicomplexan parasites. Targeting apicoplast biogenesis has the benefit of efficacy against multiple *Plasmodium* life stages and multiple pathogens. Consistent with this broad utility, antibiotics that inhibit translation in the apicoplast and disrupt its biogenesis are used clinically for malaria prophylaxis, acute malaria treatment, and treatment of babesiosis and toxoplasmosis [7, 8, 63].

Until now, a forward genetic screen for essential pathways in blood-stage *Plasmodium* has not been achieved. Previous screens in murine *P. berghei* and the human malaria parasite *P. falciparum* identified nonessential genes required for gametocyte formation [64, 65], the developmental stage required for mosquito transmission. Functional screens for essential pathways have been impeded by several technical challenges, including the low transfection efficiency of *P. falciparum*, in vivo growth requirement of *P. berghei*, and absence of efficient methods for generating conditional mutants in both organisms [28]. Nonetheless, genome-scale deletion screens in *P. berghei* and *P. falciparum* using a homologous recombination-targeted deletion library or saturating transposon-based mutagenesis, respectively, have revealed a plethora of essential genes [24, 25]. Functional assignment of these essential genes is a priority. In this context, the apicoplast biogenesis screen presented here is a major milestone towards unbiased functional identification of novel, essential genes.

A top priority for "version 2.0" is to expand the screen to genome scale, maximizing our ability to uncover novel pathways. Apicoplast biogenesis is a complex process encompassing a multitude of functions and is expected to require hundreds of gene products. The identification of 12 candidate genes and our sparse sampling of known genes suggest that the current

screen is far from saturating. The most significant bottleneck is the dependence of this screen on chemical mutagenesis. Mapping mutations by whole-genome sequencing limits the number of mutants that can be analyzed. Even for sequenced clones, less than half had a detectable point mutation in a coding region. The remaining apicoplast(−) clones may have contained mutations in noncoding regions or other types of mutations that are more difficult to detect (insertion, deletions, or copy number variations). Particularly for apicoplast(−) clones selected from non-mutagenized conditions, we considered the possibility that some parasites might spontaneously fail to inherit the apicoplast due to mechanical defects during parasite replication; these daughter cells resulting from erroneous apicoplast division and segregation usually would not survive but are rescued by IPP. Finally, specific mutations identified in candidate genes also need to be validated one by one. In this study, four nonsense mutations were validated by conditional knockdown, while a missense mutation in *Pf*FtsH1 was validated using an available activity assay. Although we were able to demonstrate loss of function as result of the *Pf*FtsH1 I437S variant, other missense mutations identified in genes of unknown function will be challenging to follow up with available genetic tools.

Given these limitations, an alternative mutagenesis method will increase the screen throughput. Options include adaptation of the *piggyBac* transposon developed for the *P. falciparum* deletion screen [25] or development of large-scale targeted mutagenesis. Switching to more genetically tractable apicomplexan organisms, such as *P. berghei* or *Toxoplasma*, would provide ready options for large-scale targeted gene disruptions [23, 24]. However, these would have to be performed under conditional regulation because chemical rescue of the apicoplast is not feasible in these organisms. We anticipate that continued advances in genetic methods in apicomplexan organisms will open up opportunities to expand this screen in the future.

Methods

Ethics statement

Human erythrocytes were purchased from the Stanford Blood Center (Stanford, California) to support in vitro *P. falciparum* cultures. Because erythrocytes were collected from anonymized donors with no access to identifying information, IRB approval was not required. All consent to participate in research was collected by the Stanford Blood Center.

Parasite culture and transfections

P. falciparum Dd2[attB] (MRA-843) were obtained from MR4. NF54[Cas9+T7 Polymerase] parasites were kindly provided by Jacquin Niles. Parasites were grown in human erythrocytes at 2% hematocrit (Stanford Blood Center) in RPMI 1640 media (Gibco) and supplemented with 0.25% Albumax II (Gibco), 2 g/L sodium bicarbonate, 0.1 mM hypoxanthine (Sigma), 25 mM HEPES (pH 7.4; Sigma), and 50 μg/L gentamicin (Gold Biotechnology) at 37°C, 5% O_2, and 5% CO_2.

For transfections, 50 μg of plasmid DNA was added to 200 μL packed red blood cells (RBCs), adjusted to 50% hematocrit in RPMI 1640, and electroporated as previously described [66]. On day 4 post transfection, parasites were selected for with 2.5. mg/L blasticidin S (RPI Research Products International). TetR/DOZI strains were cultured with 500 nM ATc for the entire duration of transfection. For TetR/DOZI strains expressing ACP$_L$-GFP or GFP-*Pf*Atg8, parasites were additionally selected for with 500 μg/mL G418 sulfate (Corning) during transfection.

Cloning

Oligonucleotides were purchased from the Stanford Protein and Nucleic Acid facility or IDT. gBlocks were ordered from IDT. Molecular cloning was performed using In-Fusion Cloning

(Clontech) or Gibson Assembly (NEB). Primer and gBlock sequences for all cloning are available in S3 Table.

To generate the plasmid pRL2-mCherry-T2A-ACP$_L$-GFP, T2A-ACP$_L$-GFP was first amplified from the pRL2-ACP$_L$-GFP vector. mCherry was amplified from pTKO2-mCherry vector (kind gift from J. Boothroyd) and inserted in front of T2A-ACP$_L$-GFP in the pRL2 backbone using the In-Fusion Cloning kit (Takara). To generate the pL2-mCherry-T2A-ACP$_L$-GFP-degron plasmids, T2A-ACP$_L$-GFP-degron was amplified from pRL2-mCherry-T2A-ACP$_L$-GFP.

For CRISPR-Cas9–based editing of endogenous Pf3D7_0518100, Pf3D7_1126100, Pf3D7_1305100, and Pf3D7_1363700 loci, sgRNAs were designed using the eukaryotic CRISPR guide RNA/DNA design tool (http://chopchop.cbu.uib.no/). To generate a linear plasmid for CRISPR-Cas9–based editing, left and right homology regions were first amplified for each gene. For each gene, a gBlock containing the recoded coding sequence C-terminal of the CRISPR cut site and a triple HA tag was synthesized with appropriate overhangs for Gibson Assembly. This fragment along with the left homology region was simultaneously cloned into the FseI/ApaI sites of the linear plasmid pSN054-V5. Next, the appropriate right homology region and a gBlock containing the sgRNA expression cassette were simultaneously cloned into the AscI/I-SceI sites of the resultant vector to generate the plasmids.

To generate plasmid for expression of GFP-PfAtg8, GFP with a GlyAlaGlyAla linker was amplified from pRL2-ACP$_L$-GFP. PfAtg8 was amplified from P. falciparum gDNA. Both fragments were inserted into pfYC110 vector [38] using the In-Fusion Cloning kit.

V. brassicaformis RNA from strain CCMP3346 was purchased from the National Center for Marine Algae and Microbiota and was subsequently used to generate cDNA using Superscript III cDNA Kit (Life Technologies). For Plasmodium PF3D7_1363700 cloning, codon optimized gBlocks were used to construct the Plasmodium construct. Constructs were cloned into the pGEXT vector using the In-Fusion Cloning kit.

Degron screening

Ring-stage mCherry-T2A-ACPL-GFP-degron parasites were treated with 10 μM actinonin (Sigma) and 200 μM IPP (Isoprenoids, LLC) to disrupt the apicoplast. Both treated and non-treated parasites were analyzed two cycles post treatment at the schizont stage on a BD Accuri C6 flow cytometer. For each condition, 100,000 to 500,000 events were recorded. Uninfected RBCs were first removed from the population by setting a gate for mCherry fluorescence. For each strain, the average GFP and mCherry fluorescence intensities were then calculated for the infected cell population using FlowJo. For example, if 10,000 infected cells were counted, then the GFP and mCherry fluorescence for each cell was measured by the flow cytometer, and the average fluorescence was determined for the whole population. To calculate the GFP:mCherry ratios for comparative analysis of degron efficiency, the GFP to mCherry fluorescence ratio for each individual infected cell was first obtained. The fluorescence ratios of all infected cells were then averaged to determine the overall population GFP:mCherry ratio.

Mutant screening

Ring-stage mCherry-T2A-ACPL-GFP-EcssrA (EcssrA) parasites were seeded onto a 96-well plate at a volume of 200 μL, 2% hematocrit, and 0.5%–1% parasitemia. Parasites were either untreated or treated with 1 mM EMS or 100 μM ENU for 2 hours, and then washed three times afterwards to remove the mutagen from the growth media. Parasites were cultured in growth media + 200 μM IPP for the duration of the screen.

At 120 hours post treatment, mutants were isolated on a Sony SH800S Cell Sorter. Uninfected RBCs were first analyzed to set the gate for overall fluorescence. Untreated *Ec*ssrA parasites were analyzed to gate for positive and negative mCherry and GFP expression, respectively. Actinonin-treated *Ec*ssrA parasites were analyzed to gate for positive GFP expression. Non-mutagenized and mutagenized parasites displaying both positive mCherry and GFP expression were FACS'd into a new 96-well plate. Enriched parasites were allowed to propagate to a detectable parasitemia before being subjected to subsequent FACS rounds.

Mutants were enriched until mCherry and GFP fluorescence approached actinonin-treated levels. In the final enrichment, up to 52 mutants were single-cell cloned. Mutants that survived single-cell sorting were split into growth media containing either 200 μM IPP or no IPP. Mutants displaying growth only in IPP were expanded to a 10 mL culture at approximately 10% parasitemia and ring-stage synchronized; 5 mL of culture was harvested for DNA extraction, and 5 mL culture was frozen at −80°C.

DNA isolation and whole-genome sequencing

Ring-stage parasites were isolated from RBC in 0.1% saponin and washed three times in PBS. gDNA from mutants and the parental strain was isolated using the Quick-DNA Universal Kit (Zymo Research). Paired-end gDNA libraries were generated and barcoded for each mutant and the parental using the Nextera Library Prep Kit, modified for 8 PCR cycles (Stanford Functional Genomics Facility). Up to 26 pooled libraries were analyzed per lane of an Illumina HiSeq 4000 using 2×75 bp, paired-end sequencing (Stanford Functional Genomics Facility).

SNP analysis

Fastq files were checked for overall quality using FastQC. Ten and 15 bp were trimmed from the 5′ and 3′ ends of all 75 bp sequence reads, respectively, to remove low-quality reads; 20 and 30 bp were trimmed 5′ and 3′ ends of 150 bp sequence reads, respectively, from an additional parental Dd2 strain sequenced by the DeRisi lab (https://www.ncbi.nlm.nih.gov/sra/SRX326518). The resulting paired-end sequencing reads were mapped using Bowtie2 against the *P. falciparum* 3D7 (version 35) reference genome. One mismatch per read was allowed, and only unique reads were aligned (reads were removed if they aligned to more than one region of the genome). PCR duplicates were removed using Samtools rmdup, and raw SNVs were called using Samtools mpileup. Indels were not analyzed.

Bcftools was used to generate the raw variant list for parental (allele frequency ≥ 0.05, depth ≥ 1) and mutant (allele frequency ≥ 0.9, depth ≥ 5) strains. Variants found in the parental strain were excluded from the mutant variant list. Variants were filtered to only include protein-coding mutations (missense and nonsense). Mutations found in hypervariable gene families were excluded. Remaining variants that were previously annotated in PlasmoDB were excluded to generate the final variant list. The reported variants were confirmed to meet the filtering requirements using Samtools tview. Mutants containing nonsense mutations were Sanger sequenced to confirm the presence of the mutations prior to genetic validation. The custom script and parameters used for analysis are available at https://github.com/yehlabstanford/biogenesis_screen.

Western blotting

Parasites were separated from RBCs by lysis in 0.1% saponin and were washed in PBS. Parasite pellets were resuspended in PBS containing 2× NuPAGE LDS sample buffer and boiled at 95°C for 10 minutes before separation on NuPAGE gels. Gels were transferred onto

nitrocellulose membranes using the Trans-Blot Turbo Transfer System (Bio-Rad). Membranes were blocked in 0.1% Hammarsten casein (Affymetrix) in 0.2× PBS with 0.01% sodium azide. Antibody incubations were performed in a 1:1 mixture of blocking buffer and Tris-buffered saline with Tween (TBST)-20 (10 mM Tris [pH 8.0], 150 mM NaCl, 0.25 mM EDTA, 0.05% Tween 20). Blots were incubated with primary antibody overnight at 4˚C at the following dilutions: 1:20,000 mouse-α-GFP JL-8 (Clontech 632381), 1:20,000 rabbit-α-*Plasmodium* aldolase (Abcam ab207494), 1:1,000 mouse-α-HA 2–2.2.14 (Thermo Fisher 26183), 1:1,000 guinea pig-α-ATG8 (Josman LLC), and 1:1,000 rabbit-α-ClpP (kind gift from W. Houry). Blots were washed three times in TBST and were incubated for 1 hour at room temperature in a 1:10,000 dilution of the appropriate fluorescent secondary antibodies (LI-COR Biosciences). Blots were washed twice in TBST and once in PBS before imaging on a LI-COR Odyssey imager.

Fractionation assay

Parasites expressing GFP-*Pf*Atg8 were grown in the presence or absence of ATc for 24 hours; 10 ml cultures were lysed with 0.1% saponin and washed 3 times with PBS. Parasite pellets were resuspended in ice-cold lysis buffer (1× PBS, 1% Triton X-114 [Thermo Scientific 28332], 2 mM EDTA, 1× protease inhibitors [Pierce A32955]) and incubated on ice for 30 minutes. Cell debris were removed by 10-minute centrifugation at 16,000 × g, 4˚C. Supernatant was transferred to a fresh Eppendorf tube, incubated 2 minutes at 37˚C to allow phase separation, and centrifuged 5 minutes at 16,000 × g at room temperature. The top (aqueous) layer was transferred to another tube. The interphase was removed to avoid cross-contamination between the layers. The bottom (detergent) layer was resuspended in 1× PBS, 0.2 mM EDTA to equalize the volumes of the two fractions. Both fractions were subjected to methanol-chloroform precipitation, resuspended in PBS containing 2× NuPAGE LDS sample buffer, boiled for 5 minutes at 95˚C, and analyzed by western blot as described above.

Microscopy

For live imaging, parasites were settled onto glass-bottom microwell dishes Lab-Tek II chambered coverglass (Thermo Fisher 155409) in PBS containing 0.4% glucose and 2 μg/mL Hoechst 33342 stain (Thermo Fisher H3570). Cells were imaged with a 100×, 1.4 NA objective on an Olympus IX70 microscope with a DeltaVision system (Applied Precision) controlled with SoftWorx version 4.1.0 and equipped with a CoolSnap-HQ CCD camera (Photometrics). Images were captured as a series of z-stacks separated by 0.2 μm intervals, deconvolved (except for mCherry images), and displayed as maximum intensity projections. Brightness and contrast were adjusted equally in SoftWorx or Fiji (ImageJ) for display purposes.

For immunofluorescence, fixed-cell imaging, parasites were first fixed with 4% paraformaldehyde (Electron Microscopy Science 15710) and 0.0075% glutaraldehyde in PBS (Electron Microscopy Sciences 16019) for 20 minutes. Cells were washed once in PBS and allowed to settle onto poly-L-lysine-coated coverslips (Corning) for 60 minutes. Coverslips were then washed once with PBS, permeabilized in 0.1% Triton X-100/PBS for 10 minutes, and washed twice more in PBS. Cells were treated with 0.1 mg/mL NaBH$_4$/PBS for 10 minutes, washed once in PBS, and blocked in 5% BSA/PBS. Primary antibodies were diluted in 5% BSA/PBS at the following concentrations: 1:500 rabbit-α-*Pf*ACP (kind gift from S. Prigge) and 1:100 rat-α-HA 3F10 (Sigma 11867423001). Coverslips were washed three times in PBS, incubated with secondary antibodies goat-α-rat 488 (Thermo Fisher A-11006) and donkey-α-rabbit (Thermo Fisher A10042) at 1:3,000 dilution, and washed three times in PBS prior to mounting in Pro-Long Gold antifade reagent with DAPI (Thermo Fisher).

Knockdown assays

Ring-stage TetR/DOZI strain parasites were washed two times in growth media to remove ATc. Parasites were divided into three cultures supplemented with 500 nM ATc, no ATc, or no ATc + 200 μM IPP. Samples were collected at the schizont stage in each growth cycle for flow cytometry analysis and western blot. Parasites in each condition were diluted equally every growth cycle for up to six growth cycles.

For parasitemia measurements, parasite-infected or uninfected RBCs were incubated with the live-cell DNA stain dihydroethidium (Thermo Fisher D23107) for 30 minutes at a dilution of 1:300 (5 mM stock solution). Parasites were analyzed on a BD Accuri C6 flow cytometer, and up to 100,000 events were recorded.

Protein expression and purification

The parent His6-SUMO-*Pf*FtsH191-612-GST plasmid as well as E249Q and D493A mutants were obtained from laboratory stocks. An I437S mutant was constructed by site-directed mutagenesis. Recombinant proteins were expressed from these plasmids and purified as described [22].

Enzyme assays

Rates of ATP hydrolysis by *Pf*FtsH1 were measured using a coupled spectrophotometric assay [67] in protein degradation (PD) buffer (25 mM HEPES [pH 7.5], 200 mM NaCl, 5 mM MgSO4, 10 μM ZnSO4, 10% glycerol) with 3% dimethyl sulfoxide (DMSO) or 50 μM actinonin in 3% DMSO at 37˚C. PD rates were measured by incubating *Pf*FtsH1 (1 μM) with FITC-labeled (2 μM, Sigma C0528) and unlabeled casein (8 μM) in PD buffer plus 3% DMSO or 50 μM actinonin in 3% DMSO. Reactions were started by adding ATP (4 mM) or buffer with a regeneration system (16 mM creatine phosphate and 75 μg/mL creatine kinase), and degradation was followed by measuring the fluorescence intensity (excitation 485 nm; emission 528 nm) at 37˚C.

Alignment of IGPS and IGPS-like proteins

IGPS and IGPS-like proteins from *V. brassicaformis* were identified by BLAST through using CryptoDB. First, secondary structure was predicted using PSI-PRED in the XtalPred suite [53, 55]. Only the sequences containing the TIM barrels of each sequence were used for alignment because there are large N- and C-terminal extensions in the noncanonical proteins. PRO-MALS3D was subsequently used to perform a multiple sequence alignment based on secondary structure and homology to proteins with determined 3D structures [54].

Bacterial complementation assay

W3110trpC9800 E. coli strain was purchased from the Yale University Coli Genetic Stock Center and were made chemically competent using calcium chloride. *BL21 Star (DE3)* competent cells (Thermo Fisher) were used for the WT condition. The competent *W3110trpC9800* cells were transformed with the pGEXT vectors containing the different *Vitrella* or *Plasmodium* IGPS and IGPS-like genes and were plated on LB agar plates containing carbenicillin. For each construct, a colony was picked and washed in M9 minimal media (M9) (22 mM potassium phosphate monobasic, 22 mM sodium phosphate dibasic, 85 mM sodium chloride, 18.7 mM ammonium chloride, 2 mM magnesium sulfate, 0.1 mM calcium chloride, and 0.4% glycerol), resuspended in M9, and streaked onto M9/agar plates containing either carbenicillin (100 μg/

mL) or carbenicillin and 1 mM L-tryptophan (Sigma). Plates were incubated at 37˚C and allowed to grow for two days, after which images of the plates were taken.

Supporting information

S1 Fig. Fluorescence assays for apicoplast reporters. (A) Flow cytometry plots showing mCherry and GFP fluorescence in untreated versus actinonin/IPP-treated parasites expressing ACP_L-GFP with no degron tag. The percentage mCherry+, GFP+ parasites in the population is indicated. Uninfected RBCs were used to set gates for mCherry and GFP fluorescence. (B) Representative live-cell fluorescent images of untreated and actinonin/IPP-treated parasites expressing mCherry and ACP_L-GFP. Hoechst stains for parasite nuclei. Scale bar 5 μm. (C) Flow cytometry plots showing mCherry and GFP fluorescence in untreated versus actinonin/ IPP-treated parasites expressing ACP_L-GFP-CcssrA or ACP_L-GFP-X7. The percentage mCherry+, GFP+ parasites in the population is indicated. Uninfected RBCs were used to set gates. (D) Average mCherry fluorescence of reporter strain populations. Data are shown as mean ± SEM (n = 3). ****P < 0.0001, unpaired two-tailed t test. Tabulated data are shown in S1 Data. (E) GFP protein levels in untreated versus IPP only, or actinonin/IPP-treated para-sites expressing GFP-EcssrA (n = 1 experiment). (F) Ratio of GFP: mCherry fluorescence in untreated versus IPP only, or actinonin/IPP-treated parasites expressing ACP_L-GFP-degron. Data are shown as mean ± SEM (n = 1 experiment). Tabulated data are shown in S1 Data. (TIF)

S2 Fig. ATc-dependent protein levels in candidate TetR/DOZI parasite strains. Individual replicates of western blot of HA-tagged protein candidates in TetR/DOZI parasite strains in +ATc, −ATc and −ATc/+IPP parasites. Protein levels for the initial and first reinvasion cycles are shown (0 and 1, respectively). Aldolase serves as a loading control. (A) Pf3D7_1126100 (Atg7), (B) Pf3D7_0518100 (conserved unknown), (C) Pf3D7_1305100 (conserved unknown), and (D) Pf3D7_1363700 (conserved unknown). (E) Individual replicates of full western blots showing ClpP processing for all candidates. (F) PCR analysis of genomic integration of TetR/ DOZI plasmid in parasite strains for each individual candidate. (TIF)

S3 Fig. Stained-gel of FtsH1 protein isolation. His_6-SUMO-PfFtsH1$_{91-612}$-GST WT and cor-responding variants were expressed from a pET22-based vector. A two-step affinity purifica-tion was performed for each recombinant enzyme (incubation and elution from Ni-NTA resin, followed by incubation and elution from GSTrap column). (TIF)

S4 Fig. Immunofluorescence localization of candidate proteins. Representative immunoflu-orescence images of Pf3D7_0518100-TetR/DOZI, Pf3D7_1126100-TetR/DOZI (PfAtg7), Pf3D7_1305100-TetR/DOZI, and Pf3D7_1363700-TetR/DOZI parasites showing colocaliza-tion of the apicoplast luminal marker ACP with 3xHA tag. Of note, lack of colocalization of Pf3D7_1363700-3xHA with ACP may be due to low protein expression. Scale bar 5 μm. (TIF)

S5 Fig. The order of PfAtg7 knockdown and apicoplast loss affects IPP rescue of growth inhibition. Growth time course of PfAtg7-TetR/DOZI parasites in absence of ATc with and without IPP. (A) PfAtg7 knockdown and IPP rescue precedes apicoplast loss in apicoplast(+) parasites. Data are shown as mean ± SD (n = 2). *P < 0.05, **P < 0.01, ***P < 0.001 compared to untreated control (−ATc black asterisks, −ATc/+IPP red asterisks), one-sample t test. Tabu-lated data are shown in S4 Data. (B) Apicoplast loss precedes PfAtg7 knockdown and IPP in

apicoplast(−) parasites. Apicoplast(−) parasites were generated via actinonin/IPP treatment. Data are shown as mean ± SD (n = 2). $^{**}P < 0.01$, $^{***}P < 0.001$ compared to untreated control (−ATc black asterisks), one-sample t test. Tabulated data are shown in S4 Data.
(TIF)

S6 Fig. Protein sequence alignment of IGPS and IGPS-like protein sequences from various organisms using PROMALS3D. Residues involved in substrate binding and catalysis (based on the *E. coli* sequence) are marked with an asterisk and are highlighted in yellow, respectively. Blue and red residues represent predicted β-sheets and α-helices respectively. All other residues have no predicted secondary structure. Highly conserved residues are represented as bold uppercase letter in the consensus line. Other consensus symbols are as follows: b: bulky; c: charged; h: hydrophobic; p: polar; s: small; t: tiny; l: aliphatic; "+": positive; "-": negative; "@": aromatic.
(TIF)

S1 Table. Amino acid sequences of degrons used for ACP$_L$-GFP reporter.
(DOCX)

S2 Table. Raw nucleotide variants identified in sequenced clones.
(XLSX)

S3 Table. Raw values for *FtsH1* enzymatic assays.
(XLSX)

S4 Table. Primers used in this study.
(XLSX)

S1 Data. Spreadsheet containing tabulated data for Figs 1C, S1D and S1F.
(XLSX)

S2 Data. Spreadsheet containing tabulated data for Fig 2C.
(XLSX)

S3 Data. Spreadsheet containing tabulated data for Fig 3B and 3C.
(XLSX)

S4 Data. Spreadsheet containing tabulated data for Figs 4B, 5B, 5E, 5H, S5A and S5B.
(XLSX)

Acknowledgments

Author Contributions

Conceptualization: Yong Tang, Katherine Amberg-Johnson, Ellen Yeh.

Data curation: Yong Tang, Thomas R. Meister, Marta Walczak, Michael J. Pulkoski-Gross, Sanjay B. Hari.

Formal analysis: Yong Tang, Thomas R. Meister, Marta Walczak, Michael J. Pulkoski-Gross, Sanjay B. Hari.

Funding acquisition: Robert T. Sauer, Ellen Yeh.

Investigation: Yong Tang, Marta Walczak, Michael J. Pulkoski-Gross, Sanjay B. Hari, Robert T. Sauer, Ellen Yeh.

Methodology: Yong Tang, Thomas R. Meister, Marta Walczak, Michael J. Pulkoski-Gross, Sanjay B. Hari, Katherine Amberg-Johnson, Ellen Yeh.

Project administration: Ellen Yeh.

Resources: Robert T. Sauer, Ellen Yeh.

Software: Thomas R. Meister.

Supervision: Robert T. Sauer, Ellen Yeh.

Validation: Yong Tang, Thomas R. Meister, Marta Walczak, Michael J. Pulkoski-Gross, Ellen Yeh.

Writing – original draft: Yong Tang, Ellen Yeh.

Writing – review & editing: Yong Tang, Thomas R. Meister, Marta Walczak, Michael J. Pulkoski-Gross, Sanjay B. Hari, Robert T. Sauer, Katherine Amberg-Johnson, Ellen Yeh.

References

1. McFadden GI, Reith ME, Munholland J, Lang-Unnasch N. Plastid in human parasites. Nature. 1996; 381(6582):482. Epub 1996/06/06. https://doi.org/10.1038/381482a0 PMID: 8632819.

2. Kohler S, Delwiche CF, Denny PW, Tilney LG, Webster P, Wilson RJ, et al. A plastid of probable green algal origin in Apicomplexan parasites. Science. 1997; 275(5305):1485–9. Epub 1997/03/07. PMID: 9045615.

3. van Dooren GG, Striepen B. The algal past and parasite present of the apicoplast. Annu Rev Microbiol. 2013; 67:271–89. Epub 2013/07/03. https://doi.org/10.1146/annurev-micro-092412-155741 PMID: 23808340.

4. Gibbs SP. The chloroplasts of Euglena may have evolved from symbiotic green algae. Canadian Journal of Botany. 1978; 56(22):2883–9.

5. Sheiner L, Vaidya AB, McFadden GI. The metabolic roles of the endosymbiotic organelles of Toxoplasma and Plasmodium spp. Curr Opin Microbiol. 2013; 16(4):452–8. Epub 2013/08/10. https://doi.org/10.1016/j.mib.2013.07.003 PMID: 23927894; PubMed Central PMCID: PMCPMC3767399.

6. Ralph SA, van Dooren GG, Waller RF, Crawford MJ, Fraunholz MJ, Foth BJ, et al. Tropical infectious diseases: metabolic maps and functions of the Plasmodium falciparum apicoplast. Nat Rev Microbiol. 2004; 2(3):203–16. Epub 2004/04/15. https://doi.org/10.1038/nrmicro843 PMID: 15083156.

7. Dahl EL, Rosenthal PJ. Multiple antibiotics exert delayed effects against the Plasmodium falciparum apicoplast. Antimicrob Agents Chemother. 2007; 51(10):3485–90. Epub 2007/08/19. https://doi.org/10.1128/AAC.00527-07 PMID: 17698630; PubMed Central PMCID: PMCPMC2043295.

8. Fichera ME, Roos DS. A plastid organelle as a drug target in apicomplexan parasites. Nature. 1997; 390(6658):407–9. Epub 1997/12/06. https://doi.org/10.1038/37132 PMID: 9389481.

9. Agrawal S, van Dooren GG, Beatty WL, Striepen B. Genetic evidence that an endosymbiont-derived endoplasmic reticulum-associated protein degradation (ERAD) system functions in import of apicoplast proteins. J Biol Chem. 2009; 284(48):33683–91. Epub 2009/10/08. https://doi.org/10.1074/jbc.M109.044024 PMID: 19808683; PubMed Central PMCID: PMCPMC2785210.

10. Kitamura K, Kishi-Itakura C, Tsuboi T, Sato S, Kita K, Ohta N, et al. Autophagy-related Atg8 localizes to the apicoplast of the human malaria parasite Plasmodium falciparum. PLoS ONE. 2012; 7(8):e42977. Epub 2012/08/18. https://doi.org/10.1371/journal.pone.0042977 PMID: 22900071; PubMed Central PMCID: PMCPMC3416769.

11. Leveque MF, Berry L, Cipriano MJ, Nguyen HM, Striepen B, Besteiro S. Autophagy-Related Protein ATG8 Has a Noncanonical Function for Apicoplast Inheritance in Toxoplasma gondii. MBio. 2015; 6(6): e01446–15. Epub 2015/10/29. https://doi.org/10.1128/mBio.01446-15 PMID: 26507233; PubMed Central PMCID: PMCPMC4626856.

12. Walczak M, Ganesan SM, Niles JC, Yeh E. ATG8 Is Essential Specifically for an Autophagy-Independent Function in Apicoplast Biogenesis in Blood-Stage Malaria Parasites. MBio. 2018; 9(1). Epub 2018/01/04. https://doi.org/10.1128/mBio.02021-17 PMID: 29295911; PubMed Central PMCID: PMCPMC5750400.

13. Sommer MS, Gould SB, Lehmann P, Gruber A, Przyborski JM, Maier UG. Der1-mediated preprotein import into the periplastid compartment of chromalveolates? Mol Biol Evol. 2007; 24(4):918–28. Epub 2007/01/25. https://doi.org/10.1093/molbev/msm008 PMID: 17244602.

14. Spork S, Hiss JA, Mandel K, Sommer M, Kooij TW, Chu T, et al. An unusual ERAD-like complex is targeted to the apicoplast of Plasmodium falciparum. Eukaryot Cell. 2009; 8(8):1134–45. Epub 2009/06/09. https://doi.org/10.1128/EC.00083-09 PMID: 19502583; PubMed Central PMCID: PMCPMC2725561.

15. Boucher MJG S.; Zhang L.; Lal A.; Jang S.W.; Ju A.; Zhang S.; Wang X.; Ralph S.A.; Zou J.; Elias J.E.; Yeh E. Integrative proteomics and bioinformatic prediction enable a high-confidence apicoplast proteome in malaria parasites. PLoS Biol. 2018. Epub September 13, 2018. https://doi.org/10.1371/journal.pbio.2005895

16. Biddau M, Bouchut A, Major J, Saveria T, Tottey J, Oka O, et al. Two essential Thioredoxins mediate apicoplast biogenesis, protein import, and gene expression in Toxoplasma gondii. PLoS Pathog. 2018; 14(2):e1006836. Epub 2018/02/23. https://doi.org/10.1371/journal.ppat.1006836 PMID: 29470517; PubMed Central PMCID: PMCPMC5823475.

17. Sheiner L, Fellows JD, Ovciarikova J, Brooks CF, Agrawal S, Holmes ZC, et al. Toxoplasma gondii Toc75 Functions in Import of Stromal but not Peripheral Apicoplast Proteins. Traffic. 2015; 16 (12):1254–69. Epub 2015/09/19. https://doi.org/10.1111/tra.12333 PMID: 26381927.

18. Fellows JD, Cipriano MJ, Agrawal S, Striepen B. A Plastid Protein That Evolved from Ubiquitin and Is Required for Apicoplast Protein Import in Toxoplasma gondii. MBio. 2017; 8(3). Epub 2017/06/29. https://doi.org/10.1128/mBio.00950-17 PMID: 28655825; PubMed Central PMCID: PMCPMC5487736.

19. Yeh E, DeRisi JL. Chemical rescue of malaria parasites lacking an apicoplast defines organelle function in blood-stage Plasmodium falciparum. PLoS Biol. 2011; 9(8):e1001138. Epub 2011/09/14. https://doi.org/10.1371/journal.pbio.1001138 PMID: 21912516; PubMed Central PMCID: PMCPMC3166167.

20. Wu W, Herrera Z, Ebert D, Baska K, Cho SH, DeRisi JL, et al. A chemical rescue screen identifies a Plasmodium falciparum apicoplast inhibitor targeting MEP isoprenoid precursor biosynthesis. Antimicrob Agents Chemother. 2015; 59(1):356–64. Epub 2014/11/05. https://doi.org/10.1128/AAC.03342-14 PMID: 25367906; PubMed Central PMCID: PMCPMC4291372.

21. Gisselberg JE, Herrera Z, Orchard LM, Llinas M, Yeh E. Specific Inhibition of the Bifunctional Farnesyl/Geranylgeranyl Diphosphate Synthase in Malaria Parasites via a New Small-Molecule Binding Site. Cell Chem Biol. 2018; 25(2):185–93 e5. Epub 2017/12/26. https://doi.org/10.1016/j.chembiol.2017.11.010 PMID: 29276048; PubMed Central PMCID: PMCPMC5820002.

22. Amberg-Johnson K, Hari SB, Ganesan SM, Lorenzi HA, Sauer RT, Niles JC, et al. Small molecule inhibition of apicomplexan FtsH1 disrupts plastid biogenesis in human pathogens. Elife. 2017; 6. Epub 2017/08/23. https://doi.org/10.7554/eLife.29865 PMID: 28826494; PubMed Central PMCID: PMCPMC5576918.

23. Sidik SM, Huet D, Ganesan SM, Huynh MH, Wang T, Nasamu AS, et al. A Genome-wide CRISPR Screen in Toxoplasma Identifies Essential Apicomplexan Genes. Cell. 2016; 166(6):1423–35 e12. Epub 2016/09/07. https://doi.org/10.1016/j.cell.2016.08.019 PMID: 27594426; PubMed Central PMCID: PMCPMC5017925.

24. Bushell E, Gomes AR, Sanderson T, Anar B, Girling G, Herd C, et al. Functional Profiling of a Plasmodium Genome Reveals an Abundance of Essential Genes. Cell. 2017; 170(2):260–72 e8. Epub 2017/07/15. https://doi.org/10.1016/j.cell.2017.06.030 PMID: 28708996; PubMed Central PMCID: PMCPMC5509546.

25. Zhang M, Wang C, Otto TD, Oberstaller J, Liao X, Adapa SR, et al. Uncovering the essential genes of the human malaria parasite Plasmodium falciparum by saturation mutagenesis. Science. 2018; 360 (6388). Epub 2018/05/05. https://doi.org/10.1126/science.aap7847 PMID: 29724925.

26. Schuster FL. Cultivation of plasmodium spp. Clin Microbiol Rev. 2002; 15(3):355–64. Epub 2002/07/05. https://doi.org/10.1128/CMR.15.3.355-364.2002 PMID: 12097244; PubMed Central PMCID: PMCPMC118084.

27. Trager W, Jensen JB. Human malaria parasites in continuous culture. Science. 1976; 193(4254):673–5. Epub 1976/08/20. PMID: 781840.

28. de Koning-Ward TF, Gilson PR, Crabb BS. Advances in molecular genetic systems in malaria. Nat Rev Microbiol. 2015; 13(6):373–87. Epub 2015/05/16. https://doi.org/10.1038/nrmicro3450 PMID: 25978707.

29. Matz JM, Kooij TW. Towards genome-wide experimental genetics in the in vivo malaria model parasite Plasmodium berghei. Pathog Glob Health. 2015; 109(2):46–60. Epub 2015/03/20. https://doi.org/10.1179/2047773215Y.0000000006 PMID: 25789828; PubMed Central PMCID: PMCPMC4571819.

30. El Bakkouri M, Pow A, Mulichak A, Cheung KL, Artz JD, Amani M, et al. The Clp chaperones and proteases of the human malaria parasite Plasmodium falciparum. J Mol Biol. 2010; 404(3):456–77. Epub 2010/10/05. https://doi.org/10.1016/j.jmb.2010.09.051 PMID: 20887733.

31. Rathore S, Sinha D, Asad M, Bottcher T, Afrin F, Chauhan VS, et al. A cyanobacterial serine protease of Plasmodium falciparum is targeted to the apicoplast and plays an important role in its growth and development. Mol Microbiol. 2010; 77(4):873–90. Epub 2010/06/16. https://doi.org/10.1111/j.1365-2958.2010.07251.x PMID: 20545854.

32. Florentin A, Cobb DW, Fishburn JD, Cipriano MJ, Kim PS, Fierro MA, et al. PfClpC Is an Essential Clp Chaperone Required for Plastid Integrity and Clp Protease Stability in Plasmodium falciparum. Cell Rep. 2017; 21(7):1746–56. Epub 2017/11/16. https://doi.org/10.1016/j.celrep.2017.10.081 PMID: 29141210; PubMed Central PMCID: PMCPMC5726808.

33. Keiler KC, Waller PR, Sauer RT. Role of a peptide tagging system in degradation of proteins synthesized from damaged messenger RNA. Science. 1996; 271(5251):990–3. Epub 1996/02/16. PMID: 8584937.

34. Gottesman S, Roche E, Zhou Y, Sauer RT. The ClpXP and ClpAP proteases degrade proteins with carboxy-terminal peptide tails added by the SsrA-tagging system. Genes Dev. 1998; 12(9):1338–47. Epub 1998/06/06. PMID: 9573050; PubMed Central PMCID: PMCPMC316764.

35. Flynn JM, Levchenko I, Seidel M, Wickner SH, Sauer RT, Baker TA. Overlapping recognition determinants within the ssrA degradation tag allow modulation of proteolysis. Proc Natl Acad Sci U S A. 2001; 98(19):10584–9. Epub 2001/09/06. https://doi.org/10.1073/pnas.191375298 PMID: 11535833; PubMed Central PMCID: PMCPMC58509.

36. Hoskins JR, Wickner S. Two peptide sequences can function cooperatively to facilitate binding and unfolding by ClpA and degradation by ClpAP. Proc Natl Acad Sci U S A. 2006; 103(4):909–14. Epub 2006/01/18. https://doi.org/10.1073/pnas.0509154103 PMID: 16410355; PubMed Central PMCID: PMCPMC1347992.

37. Hudson CM, Williams KP. The tmRNA website. Nucleic Acids Res. 2015; 43(Database issue):D138–40. Epub 2014/11/08. https://doi.org/10.1093/nar/gku1109 PMID: 25378311; PubMed Central PMCID: PMCPMC4383926.

38. Wagner JC, Goldfless SJ, Ganesan SM, Lee MC, Fidock DA, Niles JC. An integrated strategy for efficient vector construction and multi-gene expression in Plasmodium falciparum. Malar J. 2013; 12:373. Epub 2013/10/29. https://doi.org/10.1186/1475-2875-12-373 PMID: 24160265; PubMed Central PMCID: PMCPMC3842810.

39. Nkrumah LJ, Muhle RA, Moura PA, Ghosh P, Hatfull GF, Jacobs WR Jr., et al. Efficient site-specific integration in Plasmodium falciparum chromosomes mediated by mycobacteriophage Bxb1 integrase. Nat Methods. 2006; 3(8):615–21. Epub 2006/07/25. https://doi.org/10.1038/nmeth904 PMID: 16862136; PubMed Central PMCID: PMCPMC2943413.

40. Walker DM, Mahfooz N, Kemme KA, Patel VC, Spangler M, Drew ME. Plasmodium falciparum erythrocytic stage parasites require the putative autophagy protein PfAtg7 for normal growth. PLoS ONE. 2013; 8(6):e67047. Epub 2013/07/05. https://doi.org/10.1371/journal.pone.0067047 PMID: 23825614; PubMed Central PMCID: PMCPMC3692556.

41. Ichimura Y, Kirisako T, Takao T, Satomi Y, Shimonishi Y, Ishihara N, et al. A ubiquitin-like system mediates protein lipidation. Nature. 2000; 408(6811):488–92. Epub 2000/12/02. https://doi.org/10.1038/35044114 PMID: 11100732.

42. Ganesan SM, Falla A, Goldfless SJ, Nasamu AS, Niles JC. Synthetic RNA-protein modules integrated with native translation mechanisms to control gene expression in malaria parasites. Nat Commun. 2016; 7:10727. Epub 2016/03/02. https://doi.org/10.1038/ncomms10727 PMID: 26925876; PubMed Central PMCID: PMCPMC4773503.

43. Wagner JC, Platt RJ, Goldfless SJ, Zhang F, Niles JC. Efficient CRISPR-Cas9-mediated genome editing in Plasmodium falciparum. Nat Methods. 2014; 11(9):915–8. Epub 2014/08/12. https://doi.org/10.1038/nmeth.3063 PMID: 25108687; PubMed Central PMCID: PMCPMC4199390.

44. Gisselberg JE, Dellibovi-Ragheb TA, Matthews KA, Bosch G, Prigge ST. The suf iron-sulfur cluster synthesis pathway is required for apicoplast maintenance in malaria parasites. PLoS Pathog. 2013; 9(9):e1003655. Epub 2013/10/03. https://doi.org/10.1371/journal.ppat.1003655 PMID: 24086138; PubMed Central PMCID: PMCPMC3784473.

45. Tomlins AM, Ben-Rached F, Williams RA, Proto WR, Coppens I, Ruch U, et al. Plasmodium falciparum ATG8 implicated in both autophagy and apicoplast formation. Autophagy. 2013; 9(10):1540–52. Epub 2013/09/13. https://doi.org/10.4161/auto.25832 PMID: 24025672.

46. Nagano N, Orengo CA, Thornton JM. One fold with many functions: the evolutionary relationships between TIM barrel families based on their sequences, structures and functions. J Mol Biol. 2002; 321(5):741–65. Epub 2002/09/11. PMID: 12206759.

47. Jiroutova K, Horak A, Bowler C, Obornik M. Tryptophan biosynthesis in stramenopiles: eukaryotic win-
     ners in the diatom complex chloroplast. J Mol Evol. 2007; 65(5):496–511. Epub 2007/10/17. https://doi.
     org/10.1007/s00239-007-9022-z PMID: 17938992.

48. Imanian B, Keeling PJ. Horizontal gene transfer and redundancy of tryptophan biosynthetic enzymes in
     dinotoms. Genome Biol Evol. 2014; 6(2):333–43. Epub 2014/01/23. https://doi.org/10.1093/gbe/
     evu014 PMID: 24448981; PubMed Central PMCID: PMCPMC3942023.

49. Pfefferkorn ER. Interferon gamma blocks the growth of Toxoplasma gondii in human fibroblasts by
     inducing the host cells to degrade tryptophan. Proc Natl Acad Sci U S A. 1984; 81(3):908–12. Epub
     1984/02/01. PMID: 6422465; PubMed Central PMCID: PMCPMC344948.

50. Sibley LD, Messina M, Niesman IR. Stable DNA transformation in the obligate intracellular parasite
     Toxoplasma gondii by complementation of tryptophan auxotrophy. Proc Natl Acad Sci U S A. 1994; 91
     (12):5508–12. Epub 1994/06/07. PMID: 8202518; PubMed Central PMCID: PMCPMC44025.

51. Liu J, Istvan ES, Gluzman IY, Gross J, Goldberg DE. Plasmodium falciparum ensures its amino acid
     supply with multiple acquisition pathways and redundant proteolytic enzyme systems. Proc Natl Acad
     Sci U S A. 2006; 103(23):8840–5. Epub 2006/05/30. https://doi.org/10.1073/pnas.0601876103 PMID:
     16731623; PubMed Central PMCID: PMCPMC1470969.

52. Huang J, Mullapudi N, Lancto CA, Scott M, Abrahamsen MS, Kissinger JC. Phylogenomic evidence
     supports past endosymbiosis, intracellular and horizontal gene transfer in Cryptosporidium parvum.
     Genome Biol. 2004; 5(11):R88. Epub 2004/11/13. https://doi.org/10.1186/gb-2004-5-11-r88 PMID:
     15535864; PubMed Central PMCID: PMCPMC545779.

53. Jones DT. Protein secondary structure prediction based on position-specific scoring matrices. J Mol
     Biol. 1999; 292(2):195–202. Epub 1999/09/24. https://doi.org/10.1006/jmbi.1999.3091 PMID:
     10493868.

54. Pei J, Kim BH, Grishin NV. PROMALS3D: a tool for multiple protein sequence and structure alignments.
     Nucleic Acids Res. 2008; 36(7):2295–300. Epub 2008/02/22. https://doi.org/10.1093/nar/gkn072 PMID:
     18287115; PubMed Central PMCID: PMCPMC2367709.

55. Slabinski L, Jaroszewski L, Rychlewski L, Wilson IA, Lesley SA, Godzik A. XtalPred: a web server for
     prediction of protein crystallizability. Bioinformatics. 2007; 23(24):3403–5. Epub 2007/10/09. https://doi.
     org/10.1093/bioinformatics/btm477 PMID: 17921170.

56. Moore RB, Obornik M, Janouskovec J, Chrudimsky T, Vancova M, Green DH, et al. A photosynthetic
     alveolate closely related to apicomplexan parasites. Nature. 2008; 451(7181):959–63. Epub 2008/02/
     22. https://doi.org/10.1038/nature06635 PMID: 18288187.

57. Hennig M, Darimont BD, Jansonius JN, Kirschner K. The catalytic mechanism of indole-3-glycerol phos-
     phate synthase: crystal structures of complexes of the enzyme from Sulfolobus solfataricus with sub-
     strate analogue, substrate, and product. J Mol Biol. 2002; 319(3):757–66. Epub 2002/06/11. https://doi.
     org/10.1016/S0022-2836(02)00378-9 PMID: 12054868.

58. Woo YH, Ansari H, Otto TD, Klinger CM, Kolisko M, Michalek J, et al. Chromerid genomes reveal the
     evolutionary path from photosynthetic algae to obligate intracellular parasites. Elife. 2015; 4:e06974.
     Epub 2015/07/16. https://doi.org/10.7554/eLife.06974 PMID: 26175406; PubMed Central PMCID:
     PMCPMC4501334.

59. Yanofsky C, Horn V, Bonner M, Stasiowski S. Polarity and enzyme functions in mutants of the first three
     genes of the tryptophan operon of Escherichia coli. Genetics. 1971; 69(4):409–33. Epub 1971/12/01.
     PMID: 4945859; PubMed Central PMCID: PMCPMC1224543.

60. van Dooren GG, Tomova C, Agrawal S, Humbel BM, Striepen B. Toxoplasma gondii Tic20 is essential
     for apicoplast protein import. Proc Natl Acad Sci U S A. 2008; 105(36):13574–9. Epub 2008/09/02.
     https://doi.org/10.1073/pnas.0803862105 PMID: 18757752; PubMed Central PMCID:
     PMCPMC2533231.

61. Kalanon M, Tonkin CJ, McFadden GI. Characterization of two putative protein translocation compo-
     nents in the apicoplast of Plasmodium falciparum. Eukaryot Cell. 2009; 8(8):1146–54. Epub 2009/06/
     09. https://doi.org/10.1128/EC.00061-09 PMID: 19502580; PubMed Central PMCID:
     PMCPMC2725556.

62. Jomaa H, Wiesner J, Sanderbrand S, Altincicek B, Weidemeyer C, Hintz M, et al. Inhibitors of the non-
     mevalonate pathway of isoprenoid biosynthesis as antimalarial drugs. Science. 1999; 285(5433):1573–
     6. Epub 1999/09/08. PMID: 10477522.

63. Goodman CD, Pasaje CFA, Kennedy K, McFadden GI, Ralph SA. Targeting Protein Translation in
     Organelles of the Apicomplexa. Trends Parasitol. 2016; 32(12):953–65. Epub 2016/10/30. https://doi.
     org/10.1016/j.pt.2016.09.011 PMID: 27793563.

64. Ikadai H, Shaw Saliba K, Kanzok SM, McLean KJ, Tanaka TQ, Cao J, et al. Transposon mutagenesis
     identifies genes essential for Plasmodium falciparum gametocytogenesis. Proc Natl Acad Sci U S A.

2013; 110(18):E1676–84. Epub 2013/04/11. https://doi.org/10.1073/pnas.1217712110 PMID: 23572579; PubMed Central PMCID: PMCPMC3645567.

65. Sinha A, Hughes KR, Modrzynska KK, Otto TD, Pfander C, Dickens NJ, et al. A cascade of DNA-binding proteins for sexual commitment and development in Plasmodium. Nature. 2014; 507(7491):253–7. Epub 2014/02/28. https://doi.org/10.1038/nature12970 PMID: 24572359; PubMed Central PMCID: PMCPMC4105895.

66. Deitsch K, Driskill C, Wellems T. Transformation of malaria parasites by the spontaneous uptake and expression of DNA from human erythrocytes. Nucleic Acids Res. 2001; 29(3):850–3. Epub 2001/02/13. PMID: 11160909; PubMed Central PMCID: PMCPMC30384.

67. Norby JG. Coupled assay of Na+,K+-ATPase activity. Methods Enzymol. 1988; 156:116–9. Epub 1988/01/01. PMID: 2835597.